Maskless Photopatterning of Cells in Microfluidic Devices

by

Nathan Spielberg

Submitted to the
Department of Mechanical Engineering
in Partial Fulfillment of the Requirements for the Degree of

Bachelor of Science in Mechanical Engineering

at the

Massachusetts Institute of Technology

June 2015

Signature redacted

Signature of Author: _____
Department of Mechanical Engineering
May 9, 2015

Signature redacted

Certified by: _____
Anastasios John Hart
Associate Professor of Mechanical Engineering
Thesis Supervisor

Signature redacted

Accepted by: _____
Anette Hosoi
Professor of Mechanical Engineering
Undergraduate Officer

Maskless Photopatterning of Cells in Microfluidic Devices

by

Nathan Spielberg

Submitted to the Department of Mechanical Engineering
on May 9, 2015 in Partial Fulfillment of the
Requirements for the Degree of

Bachelor of Science in Mechanical Engineering

ABSTRACT

Upon examining current methods for printing and patterning of live biological cells, there is a need for a method capable of printing with the resolution of single biological cells to organize them into complex structures. In order to fill this need, building upon previous design of a dynamic lithography system, a stop flow lithography system was implemented capable of patterning individual particles with a mean accuracy of 11.92 μm and a standard deviation of 4.63 μm. This was achieved by improving the tracking capability of the software by measuring the exposure vs velocity relationship to anchor the particle as well as implementing a stop flow lithography based software approach. With the goal of producing 3D functionalized tissue, a 3D printing module was constructed for the dynamic lithography system that constructed micro-scale parts with a minimum layer height 16.42 μm of and planar resolution of 10 μm, comparable to the top available micro-scale 3D printers. To push the capability of the system, I analyzed and presented the limitations of the process via an opto-thermal model, and a computational fluid dynamics model which is then studied through a previously developed throughput analysis to get a theoretical maximum output of the system. In analyzing the limitations of the printing process, maximum input optical system power was characterized, and a theoretical maximum system throughput of 10,000 particles per second was calculated. This work is a step towards voxel based multimaterial printing, leading to printing of living artificial biological organs, better organs on a chip, or even bionic implants that combine electrical and biological elements.

Thesis Supervisor: Anastasios John Hart
Title: Associate Professor of Mechanical Engineering

Acknowledgments

Throughout the course of my career at MIT, and incredible number of people have both helped and inspired me. Many of these mentors have had impacts on both my career trajectory and the research trajectory of this project.

A great thanks goes to Professor A. John Hart for giving his students careful attention, mentorship in projects, and for helping me to define a research project for the course of my thesis. He has provided me with incredible amounts of research and career advice, for which I am extremely thankful. I am appreciative to have the opportunity to share and collaborate on the future of the 3D printing field and in particular the opportunity to work on this project.

Another special thanks goes to Dr. Ryan Oliver, for his countless number of hours spent in both mentorship and collaborative laboratory work. I am incredibly thankful for the amount of gracious time, Ryan has spent teaching me procedures and techniques, collaborating in research plans, as well as a great amount of advice he has given me.

I would also like to thank Professor Sangeeta Bhatia and Arnout Scheppers, for their help in supplying cells for experimentation.

I have been significantly supported by my family over the course of my undergraduate career, and would like to thank my father Gregg Spielberg, and mother Linda Spielberg for all of the support and life advice they have given me throughout my life and my career at MIT. They have been fundamental in encouraging me to pursue my passions for science and engineering and to them I owe my thanks. I also would like to thank my brother Jacob Spielberg for his inspiring strength which motivated me to pursue a career in research.

I would also like to thank my girlfriend Katie Bodner for her endless support during many late nights working on Psets, studying for exams, and encouragement along the way. I could not have done it without her and she has been incredible in giving me the strength and encouragement to pursue a career in research.

Contents

List of Figures

Chapter 1

Introduction

Testing drugs in animal models may not be a good precursor for human drug testing and has prompted a dire need in the pharmaceutical industry to develop more realistic human models. Organ-on-a-chip models provide a more realistic model for accurate drug testing in humans, while also providing the additional benefit of reducing the need for costly animal testing. Significant research has focused on the design and fabrication of "organs on a chip". For example, scientists have sought to mimic the function of the liver by developing livers on a chip for use in drug testing. These artificial livers are composed of a variety of cell types, acting as a set of micro-scale building blocks that can be arranged into a functional two dimensional and three dimensional patterns. Many methods such as extrusion, or microfluidic based trapping have been developed to pattern these building blocks into functional tissues, but none have demonstrated the capability to product heterogeneous cell-laden constructs with single cell resolution [1] [2]. Furthermore, many existing methods such as soft lithography based patterning, often require extensive time commitments to pattern planar features and lack inherent flexibility in the manufacturing process. Furthermore, other technologies such as dielectrophoretic patterning are able to construct complex patterns of cellular constructs, but lack the ability to construct cell laden geometries in full 3D.

In this thesis, we present the design and testing of an opto-fluidic, hardware and software based system called dynamic lithography, with the capability to construct cell laden constructs with the resolution of single biological cells or cellular aggregates.

Thesis Outline

With this motivation in mind, the goals of this thesis are to:

- Present a review of current methods of patterning / printing
- Design a system capable of arbitrarily patterning single cells or particles in 2D and 3D
- Characterize the system limits in resolution and speed
- Demonstrate the capability of printing single cells or particles in 2D

In each chapter, engineering challenges are explained that encompass the underlying goal of patterning constructs with single cell resolution.

Chapter 2 describes the current methods for patterning cells or microstructures and their limitations.

Chapter 3 describes the design of a hardware system composed of both an optical system and a mechanical system. The goal of the optical system is to provide a flexible lithography platform capable of patterning single particles. The goal of the mechanical system is to provide a high resolution platform for micro 3D printing and support of microfluidic based fabrication in 2D.

Chapter 4 describes the design of a software system utilizing computer vision based cell detection for patterning single cells in 2D and software for the patterning of 3D constructs from a 3D model.

Chapter 5 describes a fluidic system capable of delivering particles that are polymerized on demand. A model for particle aggregation and pattern generation is also proposed. Chapter 6 describes the results of patterning cells and particles in two dimensions and progress towards full three dimensional constructs. The results of micro 3D printed parts are presented as a step towards fabrication of fully three dimensional cell laden constructs.

Chapter 2

Background

The recent advancements in additive manufacturing technologies has paved the way to revolutionizing a variety of applications including high-throughput 3D-bioprinted tissue models for research, drug discovery and toxicology, high resolution models for surgery, education initiatives in the classroom, and rapid prototyping. Even though many methods in micro scale construction have been able to pattern particles in both two dimensional and three dimensional constructs, no template free discrete method for arbitrarily patterning singular particles currently exists. In this thesis, an advances on advantageous new method for patterning single particles called dynamic lithography is presented. In order to understand the impact and advantages of the dynamic lithography system, we must first examine the currently available methods for both two dimensional and three dimensional particle patterning and their observed shortfalls [1].

2.1 Previous Cell Patterning Techniques

A variety of methods have shown the ability to pattern single or groups of cells with varying degrees of success and resolution. In general, the measures to which a method is characterized or compared can be based on the methods achieved resolution, ability to retain cell viability, and ability to use biologically compatible materials [1]. The resolution of the printing systems is traditionally classified as the amount of dots or particles per inch that can be patterned by the system. In 3D printing, resolution in the planar orientation is traditionally defined as the

minimum feature size that can be patterned. Similarly in the out of plane dimension, commonly referred to as the Z dimension, the resolution is commonly referred to as the minimum stepping height or layer height of a single planar layer [1]. Another common measure of comparison in printing methods is a methods ability to keep the cells living and therefore able to grow and function. The measure of cells alive after printing compared to the number of original cells printed is encompassed in a methods measure of cell viability. The last measure of comparison between methods is the biocompatibility of materials used in the method, which has a profound impact on the cell viability.

In order to incorporate all of these metrics into two measures of comparison, we have chosen to use resolution and flexibility. In printing singular cells or particles, the resolution of the prescribed method is the singular voxel size than can range from a single cell to a 5 μm wide extruded cluster of cells. Flexibility is a combination of scaling ability of the method, number of dimension the method is capable of patterning in, and number of cell types the method can pattern. In examining the methods for printing cells as described furthermore below and shown below (Figure 1), there is a clear need for a method that is capable of patterning single cells or particles with a high flexibility. We introduce a method, dynamic lithography, capable of patterning with single particle resolution, with high flexibility from the ability to pattern multiple particle types in multiple dimensions with high scalability.

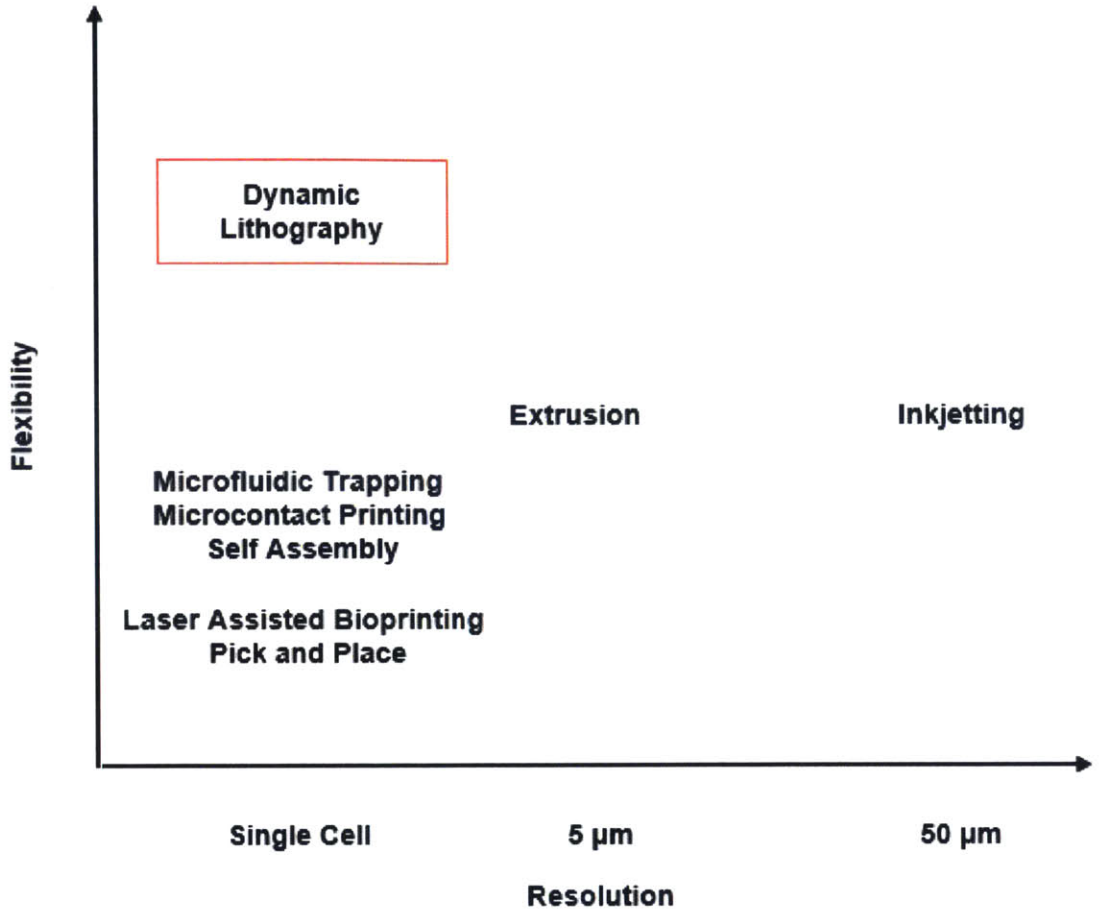

Figure 1. Comparison of cell patterning methods [1] [2] [3] [4]

2.1.1 Extrusion

Microextrusion used in the contexts of bioprinting and micro manufacturing, consists of forcing a viscous fluid containing micro particles such as cells through a small orifice or a syringe tip (Figure 2) [1]. The extruder resolution is limited by the size of the orifice through which the fluid is extruded, dictating the size of the effective filament that can be extruded. The extrusion head in a microextrusion printer is commonly mounted on a robotic Cartesian stage in order to provide movement in the x, y, and z axes. One specific advantage of microextrusion is the ability to print

many material with a wide range of viscosities due to the extrusion process. In the specific context of cells, smaller extrusion orifices lead to increasing shear in the fluid going through the orifice, which has adverse effects of cell viability. Cell viabilities observed in the microextrusion process have been observed to be less than that of the inkjet based bioprinting method with viability ranges within 40-86%. Besides decrease in viability due to shear stress at the nozzle outlet, extrusion pressure is also seen to have an effect of cell viability. Despite the decrease in cell viability, bioprinting through microextrusion has two explicit main advantages: cost and cell density. Most commercially available 3D printers contain the technology required for Cartesian motion for microextrusion which drives the cost of the method downwards. Besides this, some research groups have been able to extrude solutions solely containing cells which is desirable in some tissue engineering applications. The resolution for microextrusion methods has been shown to have a wide range, ranging from 5 μm to mm wide, depending on the size of the microextrusion orifice. Cell viability through microextrusion based methods has also been shown to have a range, ranging from 40-86%, with higher resolution due to smaller extrusion orifices generally leading to decreased cell viability [1].

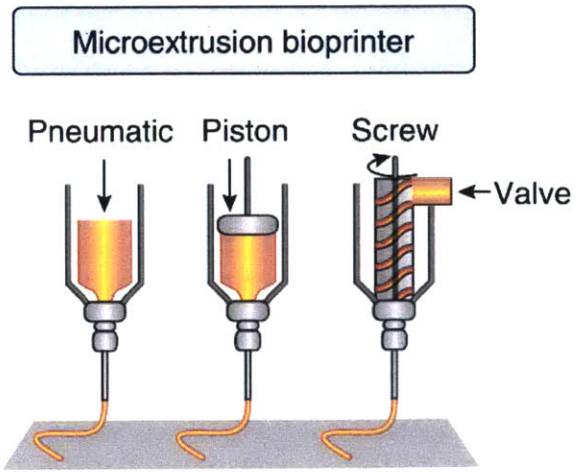

Figure 2. Examples of microextrusion printing methods [1]

2.1.2 Microfluidic Trapping

The use of microfluidic devices with prescribed patterns have been used in both active and passive methods in creating ordered arrays of particles of cells. As shown by Bhatia et al. a method for patterning cells in microfluidic devices with accuracy has been developed using dielectrophoretic forces for cell manipulation (Figure 3). In this method, first an electrode is patterning using photolithography based techniques. On thin iridium tin oxide (ITO) coated slides an insulating layer of SU-8 photoresist is used as an insulator in the photolithography process. These slides are then exposed to a mask, patterning electrically insulating features into the ITO slides. When the completed micro-patterned ITO slides are used micro channel devices, a cell solution is introduced into the device for patterning. When patterning occurs an alternating current is introduced between both top and bottom of the channel. As a result of the alternating current, the cells are pulled to the bottom of the channel in the conducting wells that are patterning as a result of the SU-8 photolithography process. After the cells are trapped in the wells in the channel, a polyethylene glycol diacrylate (PEG-DA) photopolymer solution is introduced in the channel and subsequently cured with UV exposure. As shown in the figure below patterning can be performed in a single step to generate two dimensional patterns or be performed in multiple steps with electrodes of different pattern orientations to obtain three dimensional geometries with independent layer organizations. Notable manipulation of cell clusters was observed with a resolution of ~20 μm with a channel height or effective layer height of 50 μm. Despite the advantages in ability to pattern viable cells with independent layer organization, the dielectrophoretic method requires a new set of masks, and complete photolithography steps for the product of each electrode for every single layer. Besides taking

time for making each layer, production requires the use of photolithography systems are expensive. Owing to its high use of photolithography, this method is characterized as lacking flexibility because of the need to make a new mask for every layer [5].

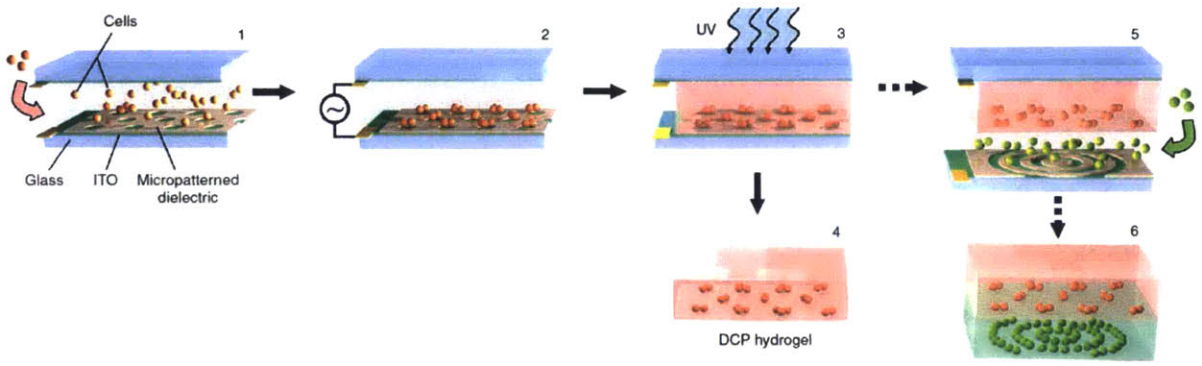

Figure 3. Dieletrophoretic patterning of cells. [5]

In addition to active microfluidic patterning, an effort to pattern cells and particles through passive means of flow in microfluidic devices has demonstrated densely packed patterned arrays of cells. In this passive means, cells are able to be positioned in a channel by being caught in flow cups patterned into the channel (Figure 4) [2]. Each cup patterned into the channel is designed to catch a single cell and allow excess fluid to continue to flow by. The microfluidic devices containing these cups are patterning with conventional soft lithography techniques and are composed of PDMS. Due to the nature of the lithography techniques, each time a new array formation is desired, a new mask, master mold, and series of devices have to be constructed. Similar to other soft lithography based methods, this method reflects poor flexibility in the manufacturing process. Patterning resolution is limited by the photolithography and soft lithography processes for the printing of the structure, whereas cell placement accuracy is dependent on the patterned structure (MF control of cell pairing and fusion).

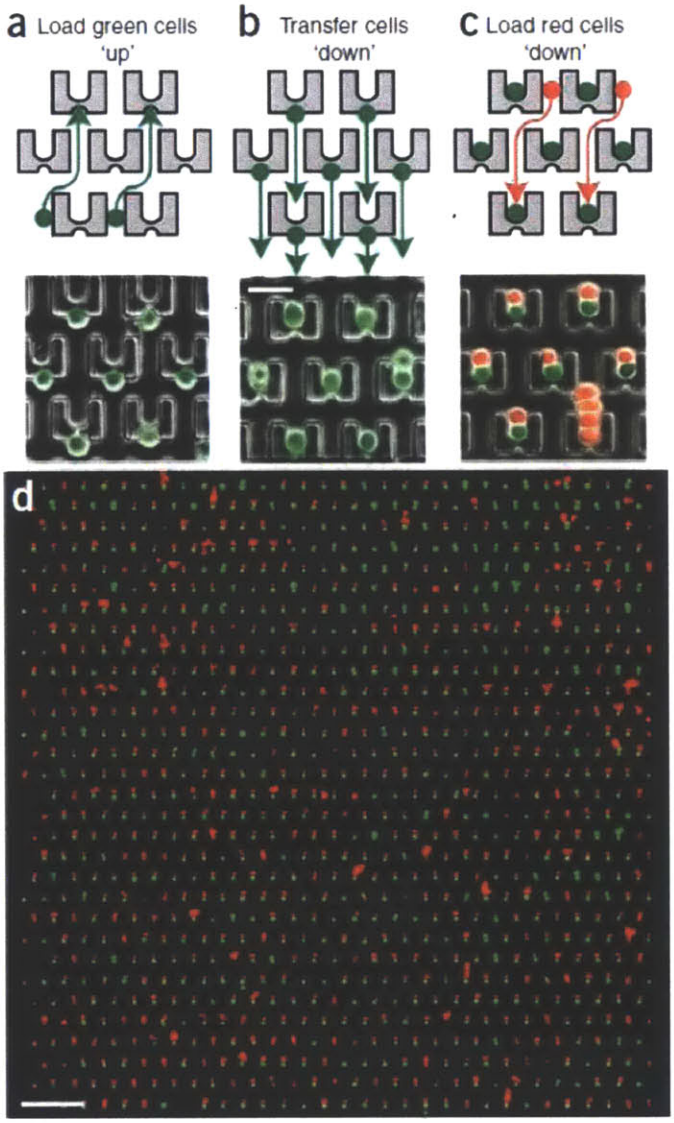

Figure 4. Template based trapping of cells in microfluidic device. a) Loading green cells by flowing one direction. b) Capturing the cells by reversing the flow. c) Loading a second red cell type flowing through the device. d) Fluorescent image of large area array of cells. [2]

2.1.3 Micro Pick and Place

Another method in the patterning and positioning of particles is the use of microelectromechanical systems (MEMS). MEMS technology has been developed by Zhang et al. with the capacity to pick and place micro-spheres with extreme, accuracy, and precision [4].

This MEMS robotic gripper used for micro-scale pick and place operation is controlled via three electrostatic comb drive actuators as shown below. Each of these microgrippers are made using deep reactive ion etching on silicon-on-insulator processing.

In manipulation and placement of the spheres, the microgripper was able to obtain positioning of 7.5-10.9 μm spheres with a release accuracy of 0.45±0.24 μm. The microgripper was able to pattern two dimensional patterns with the quoted accuracy at a rate of 6s/sphere. Owing to scaling laws, patterning of dense constructs would scale the slowest at patterning a single particle at a time, and at this method would scale at a rate of n where n is the time it takes to pattern a single particle. This method has not been tested yet for biocompatibity or capability in cell patterning, but has the potential to also perform full patterning in three dimension due to the systems build in Cartesian architecture.

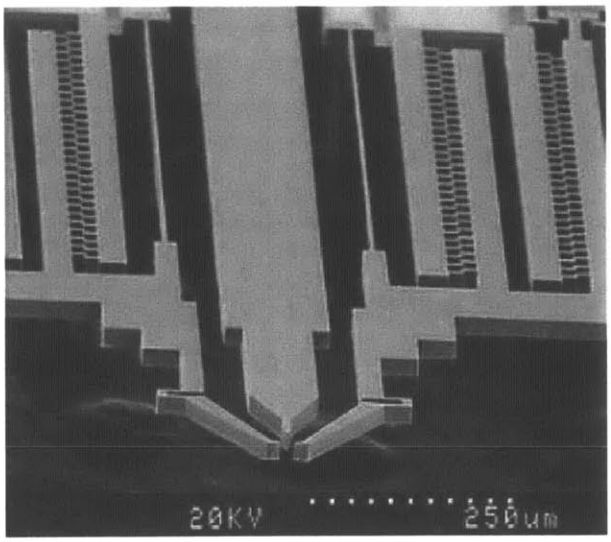

Figure 5. DRIE fabricated precision pick and place gripper. [4]

2.1.4 Autonomous Self-Assembly

Another method that is capable of producing organized constructs in both two and three dimensions is autonomous self-assembly. This method consists of fabricating cells or spheroids that undergo self-organization to assemble into organized structures with biological functionality[1]. This self-organization can also be chemically assisted as shown by Xia et al. in his soft lithography based methods of micro-contact printing and self-assembly [3]. Self-assembly has been show to create self-assembled monolayers consisting of single molecular scale or the mesoscopic scale. Resolutions in microcontact printing have been shown to achieve single line patterning below 1 μm.

Resolution in patterning is ultimately limited by the photolithography process to which the master mold is patterned for soft lithography based molding. Patterning resolution in the height direction is limited to the molecular size from the binding domain and has been shown to be as low as 2-3 nm. Despite high resolution, autonomous self-assembly requires a mask to be made for the first step in the process: photolithography of the mold. Each time a new pattern for the self-assembled monolayer is needed for a new experiment or functionality, a new mold must made through conventional photolithography and subsequent casting with polydimethylsiloxane (PDMS). Because of this photolithography step as well as the elaborate casting procedure, consisting of many steps of degassing and curing, the self-assembled monolayer method of patterning has a poor degree of manufacturing flexibility and tends to be on the higher end of the time required to pattern a substrate. The mold may be used multiple times, but in order to make a new pattern, a new mold must be made, requiring repetition of the photolithography process. Besides this, self-assembled monolayers require the steps of patterning the substrate to induce

selective binding of the monolayer often through wet etching procedures on the substrate before binding colloidal mixtures are added. Even though the method is able to obtain a singular molecular pattern on a substrate, no one has yet to adapt this method to full three dimensional tissue construction or two dimensional printing [3].

2.1.5 Inkjetting

Owing from the conventional two dimensional printing industry, another common method in bioprinting as well as 3D printing is inkjetting. Inkjet printers operate by jetting droplets of a cell stock or particle stock which consists of particles or cells dispersed in a carrier fluid. Drops are produced in inkjet printers through either thermal vapor bubbles or through piezoelectric actuation (Figure 6) [1]. In thermal actuation, small volumes of ink, or cell carrying fluid, are dispensed when a local thermal gradient at a heater expands a bubble that propels a small volume of fluid of the inkjet printing head. In the piezoelectric inkjet case, a piezoelectric crystal in the inkjet head oscillates given an applied voltage, propelling small volumes of ink out of the printer head.

Even though in thermal jetting, the heating element increases to temperatures of 200-300 $^{\circ}$C, the time scales of exposure in biological inks are small enough to not cause decreases in cell viability [1]. In both cases, the inkjet heads are attached to Cartesian motion stages to provide manipulation in x, y, and z space. One advantage on inkjetting is its wide availability from use in most commercially available office printers, driving the cost of inkjet heads down and increasing accessibility. Droplets can be ejected up to 10,000 times per second with volumes ranging from 1-300 pl. One disadvantage is that to facilitate droplet formation in the inkjet heads, often low

concentrations (less than 10 million cells/ml) are used in biological inks. Inkjet bioprinters often use hydrogels are the carrier material in the ink, using photo crosslinking or chemical methods for gelation. Even though each droplet is small in volume, due to observed surface effects the resolution of the droplet size is 50 μm wide. Cell viability on average is higher than microextrusion based methods with a viability of 85%, however single cell and precise mixtures of cells and precise mixtures of cells and functional additives have not been achieved. Positioning resolution of each droplet is a function of the Cartesian stage the inkjet head is mounted on.

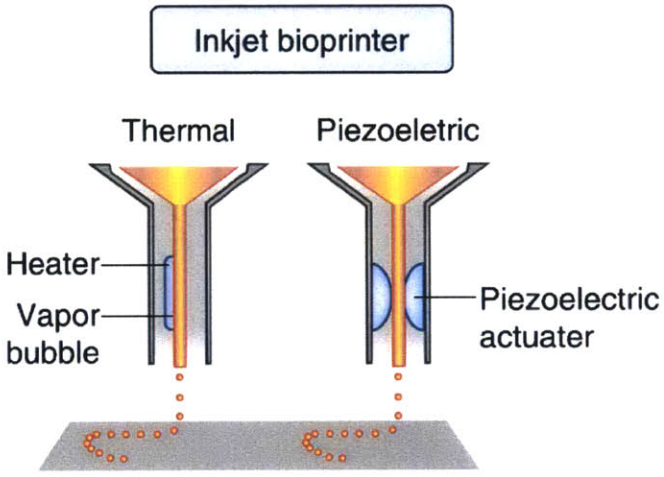

Figure 6. Mechanism for inkjet printing of cells and particles. [1]

2.1.6 Laser Assisted Bioprinting

Laser assisted bioprinting, often referred to as LAB, operates based on the principles of laser-induced forward transfer [1]. LAB systems often contain a pulsed laser, focusing system, a transfer glass usually composed of a slide with a laser energy absorbing layer with a layer of biological material coated on the bottom (Figure 7). Similar to thermal ejection in ink based jetting of biological materials, the pulsed laser in LAB is focused on the donor slide and upon

incidence with the thermal absorbing material causes local heating, ejecting small droplets of biological material onto the downward facing substrate. LAB has been used to pattern cells with densities up to 10^8 cells/ml with micro-scale resolution of down to single cell resolution with focusing optics. LAB has been able to operate with pulse laser speeds of up to 5 kHz leading to printing rates of up to 1,600 mm/s. Even though LAB is both high speed and high resolution, the preparation of each donor slide if often very time consuming and requires elaborate process preparation. Because of the difficulty of obtaining a uniform cell coating on the surface of the donor slide, targeting single cells for printing is difficult using LAB, even though efforts are being developed to include cell recognition and scanning into the LAB process. Because of their pulsed lasers, and focusing optics, LAB systems are often very high cost compared to extrusion and jetting technologies. It is still unclear whether LAB technologies can be scaled for use in constructing larger cellular constructs or for creating three dimensional patterns as only small two dimensional patterning has been demonstrated.

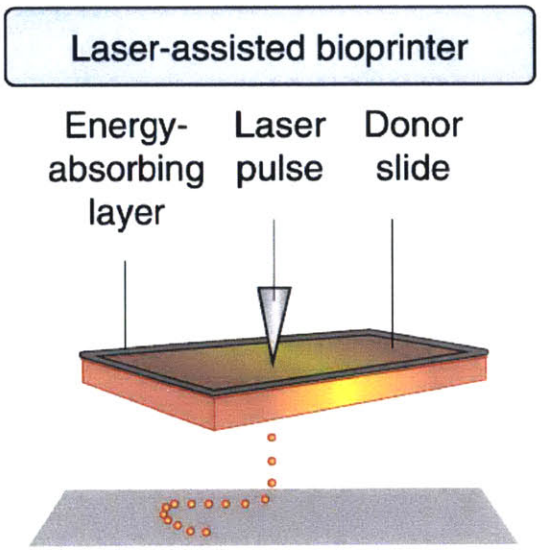

Figure 7. LAB based printing schematic. [1]

2.1.7 Microcontact Printing

Microcontact printing is a set of techniques that operate by using stamps based on PDMS soft lithography [3]. In microcontact printing, a master mold make through using conventional photolithography techniques is patterned. When making a pattern, a silicon wafer is first coated with photoresist and then selectively exposed with a set of master masks (Figure 8). Upon washing, this procedure leaves a defined pattern in the silicon wafer that can be used as a mold for the PDMS replica. This mold is then used to cast PDMS in, and then cured in a vacuum chamber. Once the PDMS replica of the mold is cured, it can be used for microcontact printing. Printing occurs when the stamp is coated with a polymeric or ink material and then placed on a substrate. Depending on the type of microcontact printing, rollers can be used for large area printing as shown in Fig. Microcontact printing of chemical for wet etching substrates is often the first step in the procedure of formation of self-assembled monolayers as described above. PDMS molding is able to obtain resolutions of less than 1 μm with singular layer heights as low as 2-5 nm. Even though high resolution and effective, microcontact printing lacks the flexibility of traditional methods for printing such as inkjet, extrusion, or LAB methods because of the need to make a master mold and replica for every new pattern [3].

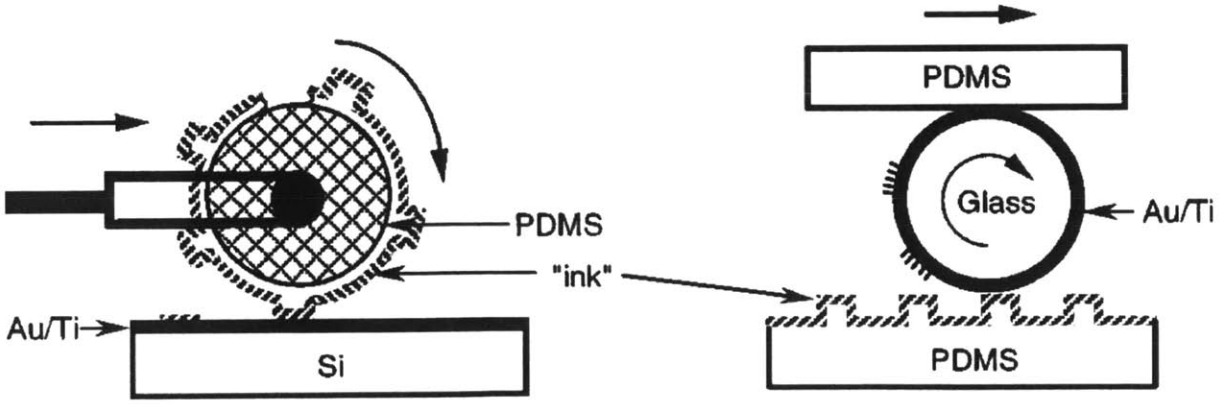

Figure 8. Schematic of microcontact printing. [3]

2.2 Stop Flow Lithography

In photopatterning two dimensional constructs of both particles and cells, dynamic lithography leverages the microfluidic design methods of stop flow lithography. Stop flow lithography is a class of lithography methods for fabrication of microparticles in a microfluidic channel (Figure 9) [6]. During stop flow lithography a photopolymer is pumped through a microfluidic device. The nominal state of the photopolymer is a liquid and upon exposure to a pattern of light, the photopolymer cures. Poly(etheylene glycol) diacrylate is the photopolymer used and it has been established oxygen inhibits its polymerization. Oxygen diffusion through the PDMS microfluidic channel therefore inhibits photopolymerization of the microparticles near the channel surface so that the particles remain free floating. Since the polymerization is constrained to the channel, particles can be made via photolithography and then subsequently flowed out of the channel with a pressure source at the inlet. The combination of flowing polymer into the channel, photolithography to make particles, and then subsequent flow to move the particle out of the channel is a repetitive high throughput process denoted at stop flow lithography [6].

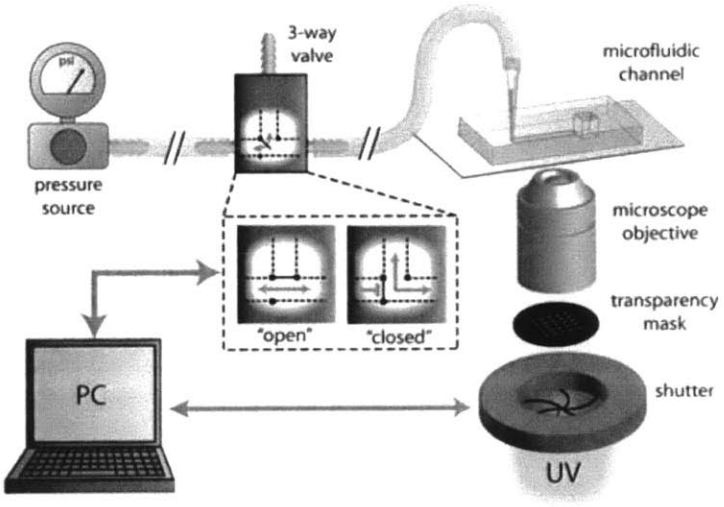

Figure 9. Schematic of the stop flow lithography process. [6]

2.3 Micro-Scale 3D Printing

Micro-scale 3D printing is a class of techniques designed to construct three dimensional objects at the micron scale. In the dynamic lithography methods, the focus of micro-scale 3D printing is on lithography, a technique that uses light as a means to construct objects. In lithography based 3D printing technique, a photopolymer or polymer that can be cured when hit by a specific wavelength of light due to free radical polymerization, is used as a building material for the 3D printed parts. In building three dimensional parts, each layer or vertical slice of the three dimensional part is cured, one at a time. The first exposed layer is often adhered to a build platform that has the ability to move in the vertical direction. After each layer is subsequently cured, the build platform moves either upwards or downwards in order to allow more photopolymer to be exposed for the next layer through flow from displacement of the build platform. After a successive set of exposures and motion, a three dimensional part is created. A key component of lithography based 3D printing is the ability to have a selective exposure in each layer. In many lithography based printers this is accomplished with either a scanning laser or with a Digital Light Processing Array (DLP). In direct write stereolithography, as seen below in Figure 10a the printer consists of a resin bath containing the photopolymer, a build stage capable of moving in the vertical direction and a direct write scanning laser capable of photopolymerizing the polymer. In the direct write setup, the build platform progresses downward in the vertical direction further into the resin bath, indicating that the polymerization occurs at the air polymer interface. In inverse stereolithography, the scanning laser or DLP based technology is located under the build platform as shown below in Figure 10b. In this case, the

build platform progresses out of the resin tank, indicating that the build interface is between the resin at the bottom of the tank and the bottom surface of the build platform. PDMS is often used at the bottom of these inverse stereolithography resin tanks in order to inhibit photopolymerization on the bottom surface of the tank [7]. Various parts printed through this process as well as extrusion are shown for reference below in Figure 11.

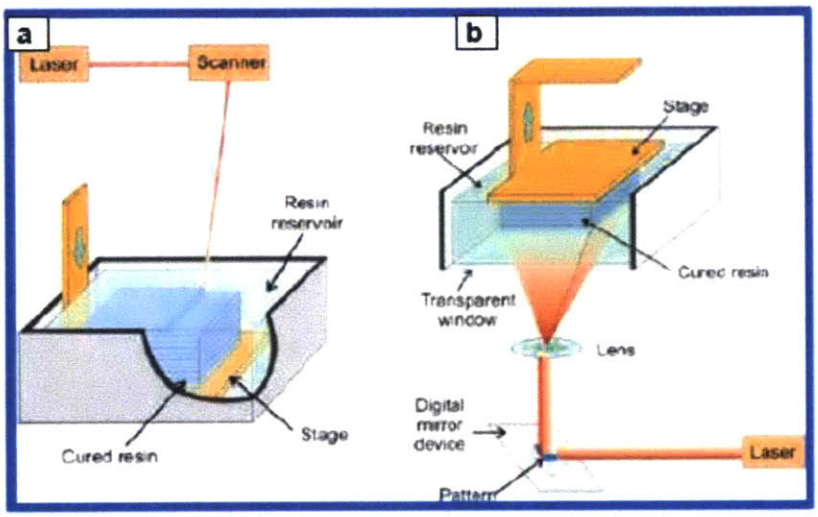

Figure 10. Direct write stereolithography. [7]

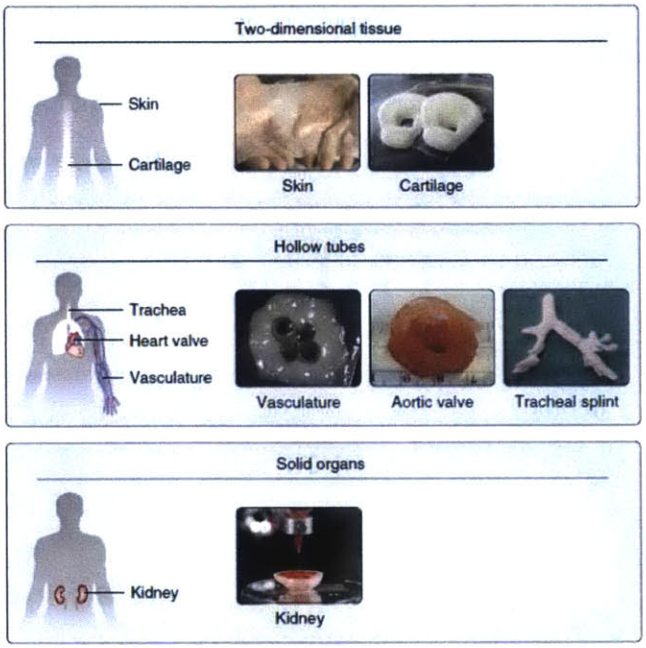

Figure 11. Examples of various parts made by 3D bioprinting [1]

2.4 Previous Work in Dynamic Lithography

In previous work by Dr. Ryan Oliver, a flexible lithography system, termed dynamic lithography was created with the ability to enable a large increase in flexibility in the photolithography process at high resolution scales. The dynamic lithography system leverages both recent advances in the hardware of lithography and inverse stereolithography based 3D printing as well as advances in optics and imaging that allow for accurate particle positioning and encapsulation [8] [6] [7]. Moreover, modern computing power enables real time image analysis of the video to dynamically change the projection in response to particle identification by the system.

2.4.1 Optical System Design

In designing an optical system with the capability to photopolymerize free radical based polymers, we have chosen to forego traditional lithography based designs. Traditional lithography systems use a fixed mask, which is used to pattern photoresists. In many of the previously shown methods such as stop flow lithography, and microcontact printing, a fixed mask or set of masks are used which broadly limits the flexibility of the manufacturing process. Instead of having a fixed set of masks, we have designed an optical system that can project any specified mask, enabling a flexible photolithography process. Because of this flexibility, the system can forego some of the problems with conventional lithography processes, such as the time required in making masks for lithography or making molds in conventional PDMS molding for microcontact printing. To obtain this flexibility, at the heart of the system we have integrated a Digital Micromirror Device (DMD) chip as shown in Figure 12 as originally invented by Larry Hornbeck of Texas Instruments [9].

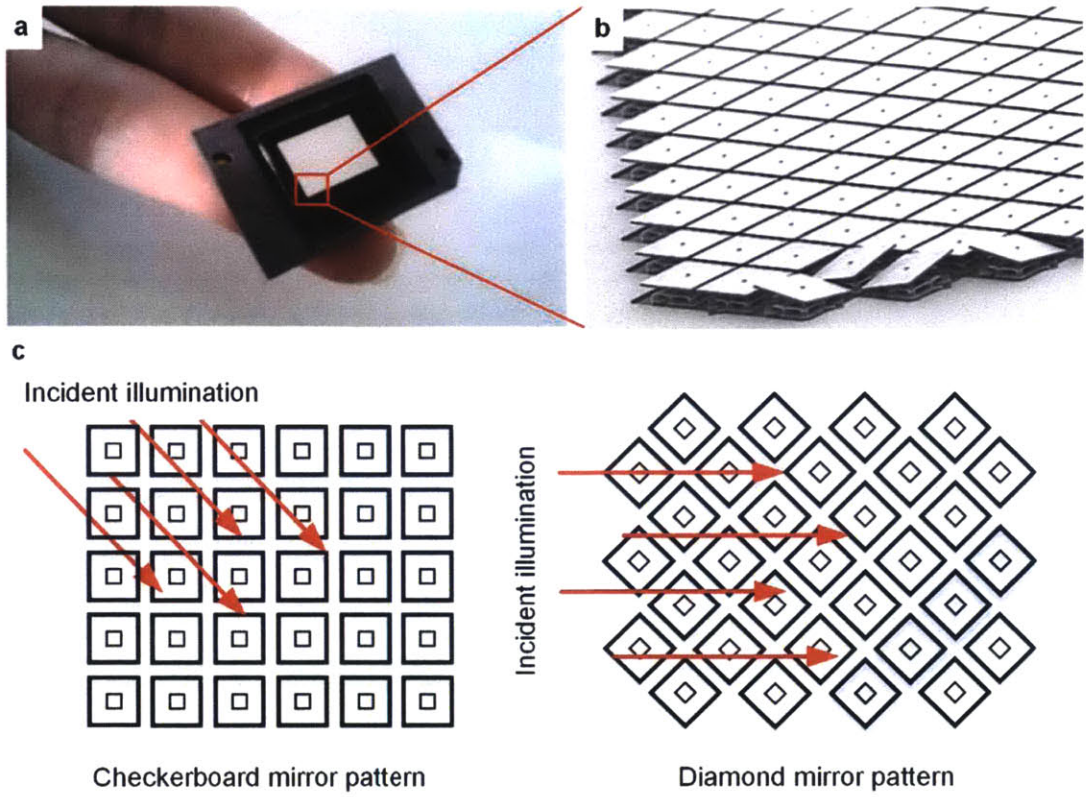

Figure 12. DMD design and configurations. a) Photograph of the DMD chip and housing. b) SEM of DMD micromirrors. c) Checkerboard mirror pattern. d) Diamond mirror pattern. [10]

A DMD chip is a micro-electro mechanical system (MEMS) that consists of an array of individually addressable micro mirrors. This system of mirrors creates an image by selectively reflecting incident light on the micromirrors. As shown in Figure 12b, the micro mirrors selectively reflect light by rotating about a built in hinge at the base, by means of an electrical signal [9]. Each mirror in the DMD, can be addressed as an individual pixel and when light is shined upon the DMD, by addressing each individual pixel an accurate projection can be created. This projection can then be used as a stand in for a mask in the photolithography process.

Besides the flexibility in determining a pattern to be projected on the substrate, in tracking particles we have chosen to integrate a charge coupled device (CCD) camera in the optical path

in order to provide optical feedback during the photolithography process. By integrating a CCD in the optical path, we have the capability of imaging or taking video of the photolithography process as it occurs, gaining valuable insights on the polymerization process, as well as having the ability to close the loop in lithography processes. Particularly, using the CCD in conjunction with tracking computer vision algorithms, enables particle tracking and analysis which is explained in depth in the software section. To utilize both the DMD and the CCD many optical elements are implemented into the optical path such as a beam splitter shown in Figure 13. Lastly, the image is focused down on the sample using an objective, which is at its simplest like a large magnifying lens with a short focal length. By using an objective in combination with the CCD and DMD, we are able to both image and project at small length scales. By doing so, we can polymerize particles in place with high resolutions as characterized below [8].

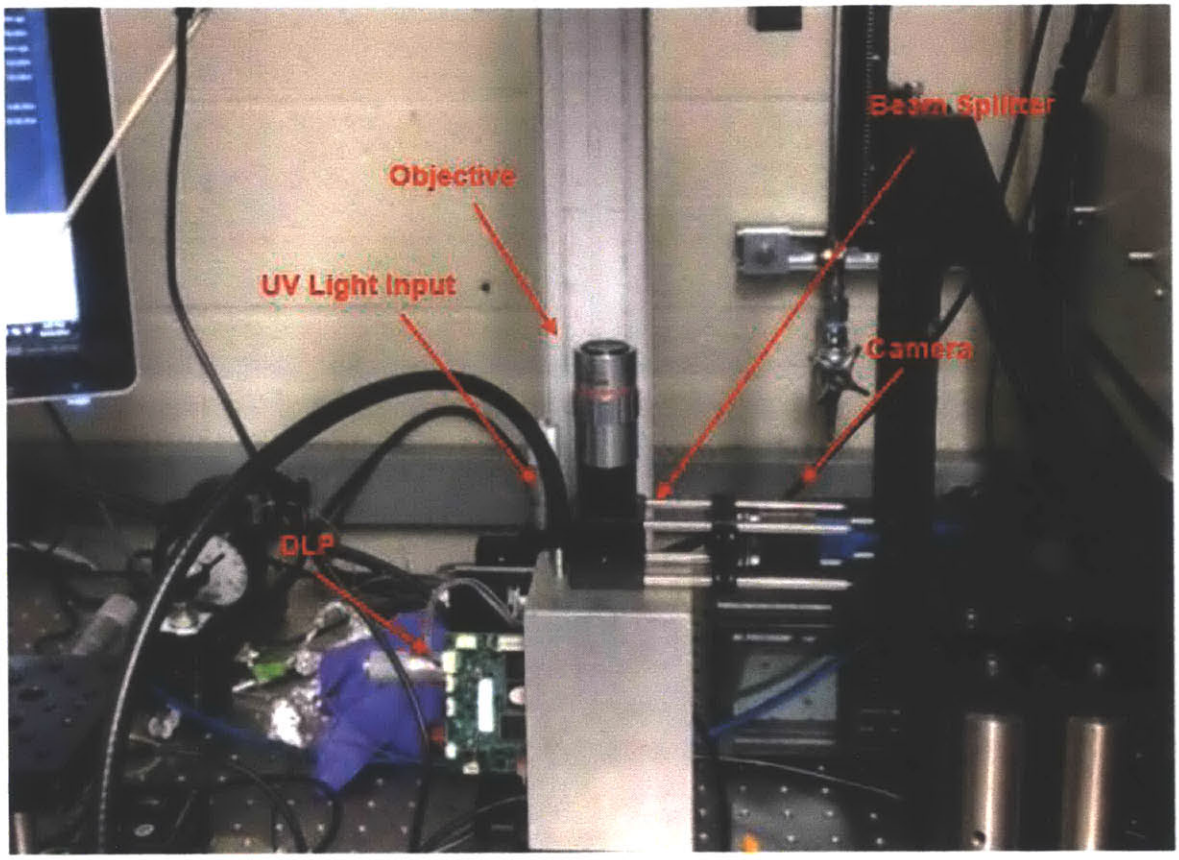

Figure 13. Dynamic lithography system overview.

In the planar projection direction, the minimum feature size is characterized by the optical capabilities of the dynamic lithography system. In previous characterization of the optical resolution, performed by colleagues Ryan Oliver and Adam Stevens, in curing hydrogel polymers a USAF 1951 test target was tested by projection on a glass substrate with polymer on it as shown below in Figure 14. Using PEG-DA, as used in the encapsulation experiments, a minimum resolution of 10 μm was achieved [8]. A higher resolution was achieved by using a different MicroChem resist, with a measured resolution of 5 μm for a 5 μm thick layer.

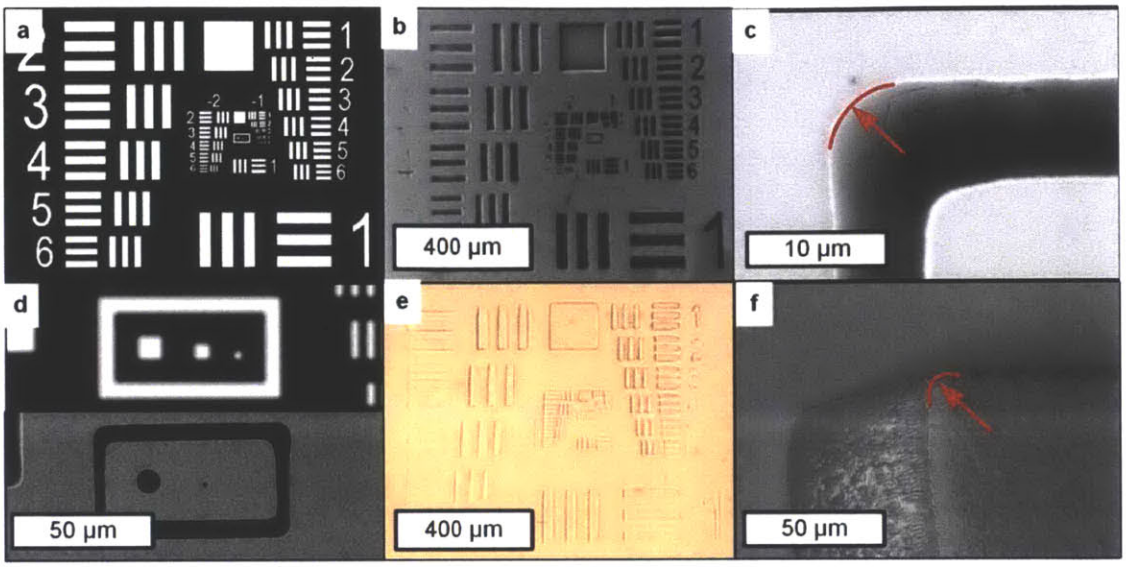

Figure 14. Resolution limits of system using 5X objective. a) USAF 1951 test pattern. b) Test pattern projected into 5 um thick layer of MicroChem resist. c) Close up view of the corner radius of box shown in (d). d) The smallest features projected and the resulting curving to the feature corners. e) The same USAF pattern in PEG-DA. f) The corner radius as of the small box as shown in PEG-DA. [8]

2.4.2 Software System Design

In printing of two dimensional arrays of particles, we have demonstrated a technique of printing by encapsulation. In this technique, particles surrounded by photopolymer flow in a microfluidic channel. Since the particles are fully encompassed in polymer, when they are at a desired location as specified by a mask or desired final 2D pattern, they are anchored in place through photopolymerization using the dynamic lithography optical system. As discussed by Oliver, due to the shallow depth of field and high contrast, thresholding can be used to find the centroids of each particle in the image [8]. Their motion is predicted using a Kalman filter to correctly position the projection accounting for latency in the computing and imaging system. Building on this work we algorithm which a. chooses when a particle is in the correct location and b. determines the order to pattern particles is improved upon and described.

In this anchoring process, there are two viable software methods which we have coded and characterized. The first method is called dynamic lithography, which is shown in Figure 15 below.

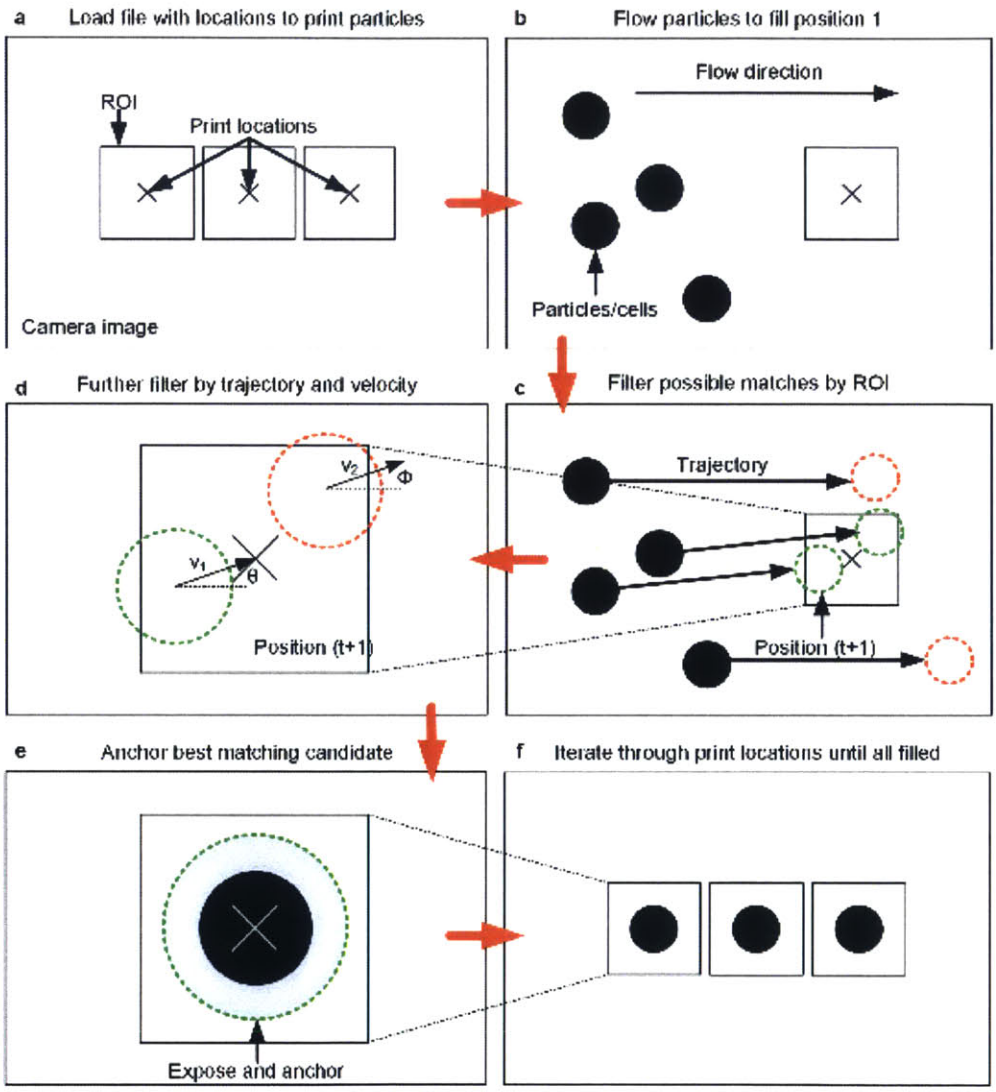

Figure 15. Printing process overview. a) Load in the print locations from file. b) Flow particles across the device. c) Identify particles that are close to the print location. d) Select only the best particle. e) Anchor the particle by exposing a mask onto it. f) Repeat this process for all print locations. [8]

In dynamic lithography, the particles are anchored or polymerized in place as they are flowing in a microfluidic device. First in the dynamic lithography, the user specifies a mask or a two dimensional pattern that they want to fill in with particles. Next the software uses an algorithm to place particle print locations within the mask as shown resulting in Figure 15a. In order to know when the particle is over or near a print location so it can perform photopolymerization and anchor the particle in place, the software has select locations where it performs computer vision operations called regions of interest (ROI). After the particle print locations are established, select ROIs around those print locations are calculated in software. Once the initial print locations and regions of interest are calculated, flow is initialized in the channel by sending a digital signal to a valve. Once flow is initialized, in dynamic lithography the software can begin checking for matching particles. During the course of the printing process, these ROIs are then checked to see if the particle is a match for each print location as shown in Figure15c. In order to see if the particle is a match, the software estimates the angle of attack of the particle as well as the particle velocity in order to determine both when and if the particle will land in the desired print locations. If either of these conditions lead to a match in print location, when the particle flows over the location, it will be photopolymerized by the software and anchored in place at the specified print location as shown in Figure15e. Lastly, this process is repeated throughout the course of flow until the whole array is completely filled up as shown in Figure15f.

Limitations in this method motivate the switch to a similar but new method using the same hardware, but based on stop flow lithography as shown above. In polymerizing the particles during the flow process, often particles are missed due to the lateral differences in velocities of particles or differences in curing dynamics as the particles are being anchored. In order to obtain

higher accuracy in system patterning, a simplified version of the dynamic lithography process is used, based off of stop flow lithography.

2.4.3 Dynamic Lithography Performance

In previous work using dynamic lithography by Ryan Oliver and Lily Chin, polystyrene (PS) beads were patterned in both an arrayed formation as well as an arbitrary pattern: the MIT logo [8]. As shown in Figure 16, patterning with PS beads successfully demonstrate the capability to anchor with single particle resolution in both arrayed and arbitrary configurations but also demonstrate areas for improvement even though this implementation does not include a tuned Kalman filter algorithm. The 2x2 matrix of printed beads is shown in Figure 16a while the MIT pattern is shown in Figure 16b.

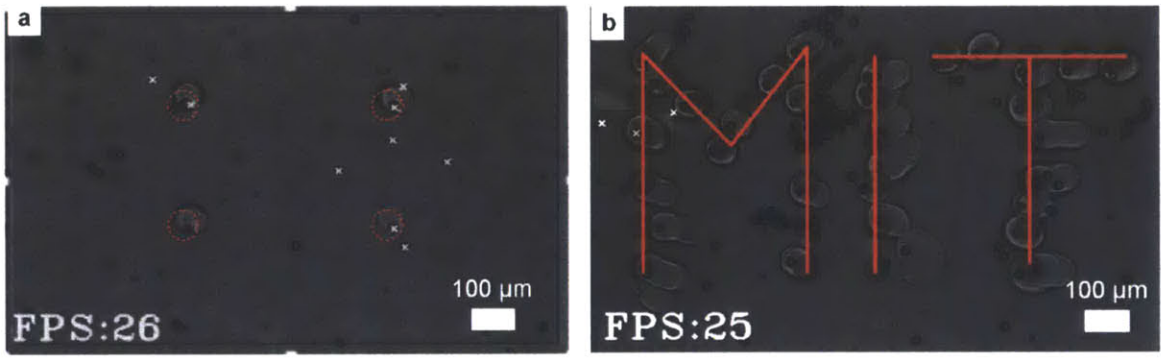

Figure 16. a) 2x2 pattern of particles. b) Attempt to pattern the words MIT from individual particles. [8]

As shown above, particles are shown to be anchored with an average of 22 µm with a standard deviation of 2.5 µm from the desired print location. Even though the particles are encapsulated, the shape of the polymerized locations is often not perfectly circular in encapsulating the particles. When using IPS cells this could lead to device clogging as the hydrogel would not

prevent the cells from growing until the filled the entire channel. Moreover the polymerized area is over 2X larger than the particle, as shown in the MIT logo, trailing polymerization locations are observed. These trailing locations increase the amount of hydrogel that encapsulates the particle, hence increasing the distance for mass transport and diffusion, making it harder for printed cells to remain viable. Ideally, in encapsulating cells, cells will be anchored with the least amount of hydrogel around them as possible in order to anchor them but still allow the free ability for mass transport and diffusion, hence increasing viability. We hypothesize that an increased understanding of variation in polymerization behavior and kinetics can help in leading to identifying the source of error in the variation of polymerization in particle flow as shown by the trailing in future iterations of the dynamic lithography software.

Other opportunities for improvement are shown in the aggregation of particles in the printing process, that complicate tracking and printing algorithms. The clumping as observed in the MIT logo leads to inaccuracies in printing, such as deviations from normal flow of particles, clogging of the microfluidic channel, and blocking of print locations. For these reasons, we have chosen to attempt to increase the accuracy of the system through simplification of the dynamic lithography method. In an attempt to simplify the dynamic lithography process, we have chosen to pursue a stop lithography based approach, where there is less need to accurately characterize the polymerization dynamics as particles are moving while being polymerized. In order to characterize and subsequently maximize the speed of the system, we must first conduct a power analysis of the system with the optics previously discussed in mind [8].

Chapter 3

Design and Modelling of the Cell Printing System

3.1 System Power and Analysis

In order to improve upon previous work on the system as well as optimize the system for a maximum throughput in patterning particles, an opto-thermal model is developed. This model helps in specifying an optimal input system power to decrease the time to cure photopolymer without damaging the system. A thermal analysis is used to ensure viable materials such as cells are not damaged by incident radiative heating.

3.1.1 Modelling of Power and Heat Transfer

In order to characterize system limitations in patterning speed as well as system performance in patterning particles, a model is necessary. First, an empirical model of the polymerization is composed by using a combination of the standard stereolithography working curve and polymer curing characteristics as notes by Tumbleston et al [11].

Using the working curve Equation 1, the polymerization characteristics of the resin are able to be estimated by measuring the curing energy and exposure time over a standard gridded test pattern. The total resin absorption coefficient (α), the resin curing dosage (D_{c0}) can be fitted given empirical data from a known time t, and radiant flux (ϕ_0) [11].

$$Cured\ thickness = \frac{1}{\alpha}\ln(\frac{\phi_0 \alpha t}{D_{c0}}) \qquad \text{Equation 1}$$

In creating an empirical test grid, illumination power is varied from values of 0.497 mW to 1.57 mW and measured using a Thorlabs PM100D optical power meter. Upon measuring power, the projection area is then measured using ImageJ, in order to get an estimation of the power per unit area used in photopolymerization. The scale of the image measured was calibrated using a calibration slide when projecting over the whole projection area.

The measured power P is then converted to radiant flux ϕ_0 , using Equation 2, where λ is the dominant wavelength of light used for polymerization, h is Plank's constant, and c is the speed of light.

$$\phi_0 = \frac{P\lambda}{hc} \qquad \text{Equation 2}$$

When empirically performing the arrayed test grid, the dynamic lithography system is programmed to perform a set of gridded exposures with exposure times ranging from 0.1 to 21.1 seconds. After exposing the full test grid array on a glass slide, the heights of each pillar on the

array were measure optically on a Zeiss microscope as shown in Figure 17a. By measuring the heights and knowing the power as well as exposure time, an experimental fit is shown in Figure 17b. By fitting this empirical model, the resin parameters can be found to be $\alpha = .016$, and $D_{c0} = 1.08 * 10^{16}$.

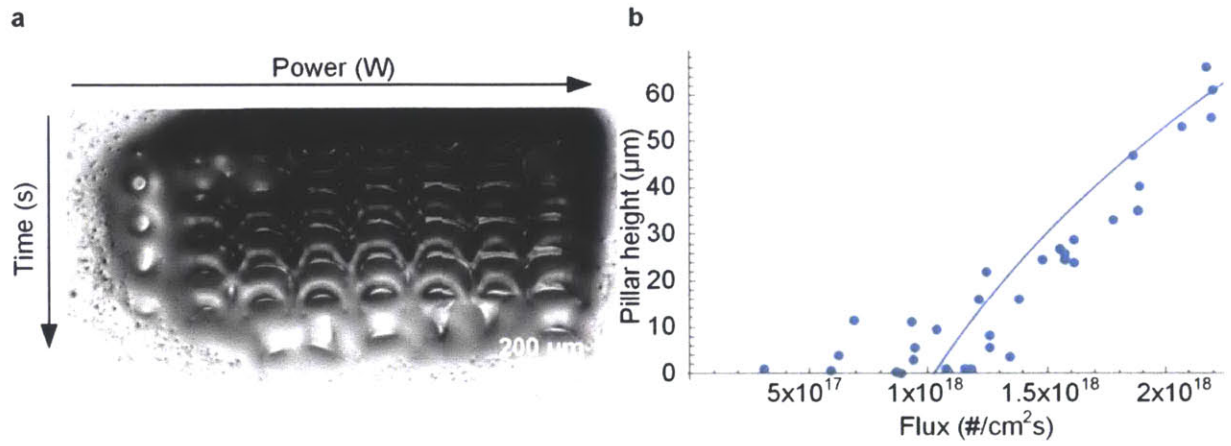

Figure 17. Array test pattern. a) Exposures in PEG-DA formulation for cell patterning while changing power and exposure time. b) The measured resulting pillar height for the flux values tested.

Once the resin parameters are deduced, the power can now be calculated to cure a 200 µm layer of polymer in a given exposure time. The cure depth used is 200 µm, as it is the channel height of the microfluidic devices used in the dynamic lithography system. The power is then plotted as a function of exposure time as shown in Figure 18.

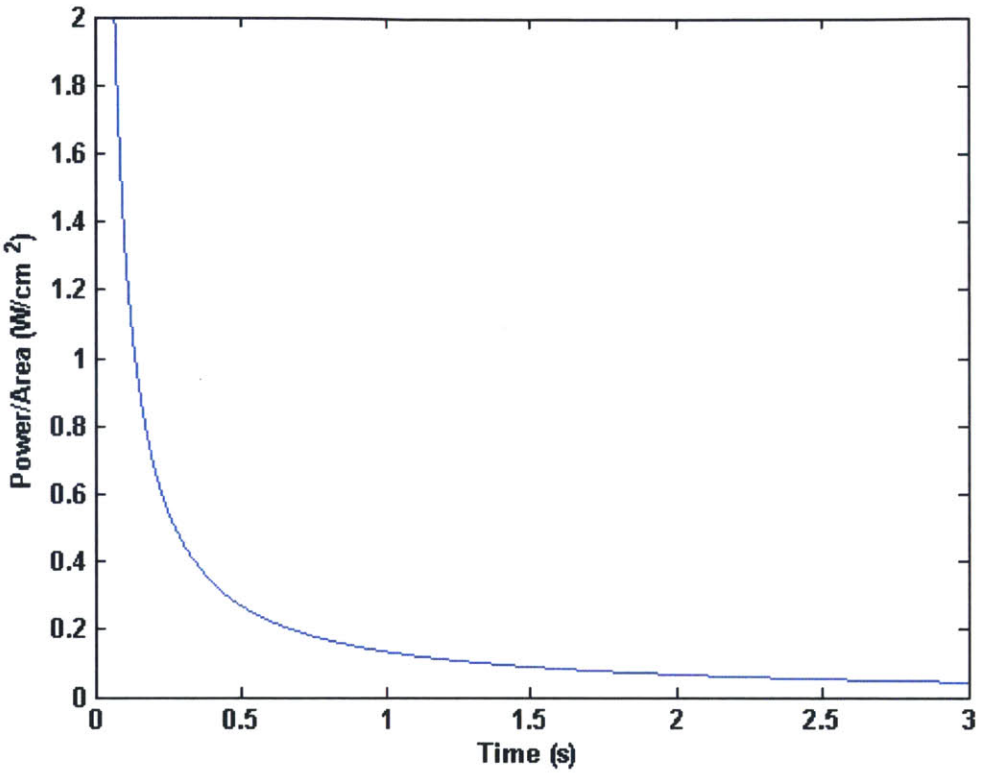

Figure 18. Calculated power required to polymerize 200 μm plotted against time.

In taking into account the curing power as shown above in Figure 18, this is the power as measured at the surface of the polymer. In order to obtain a greater idea of the limitation of the system, a better estimate of the required power is the power of the light at the light source. In order to understand how the power changes through efficiency losses along the optical train in the dynamic lithography system, a model and accompanying measurements are shown in Figure 19.

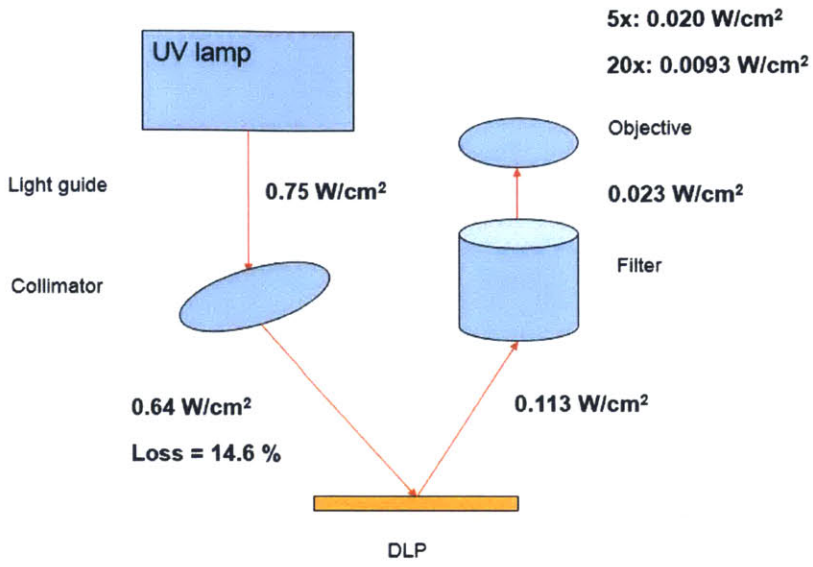

Figure 19. Schematic showing efficiency loss through the lithography optical train.

By measuring the power at the input as well as the output, we can obtain an optical efficiency (η) loss that couples the projected power to cure the polymer as specified by the polymer model in Equation 3 to the system specified input power which is a design criterion.

$$\eta_{optics} = \frac{Output\ Power\ with\ 5x\ Objective}{Input\ Lamp\ Power} = 0.027 \qquad \text{Equation 3}$$

Besides the input power loss due to light passing through the system optics, there is also an optical efficiency loss in passing through the microfluidic devices used in polymerization. In the inverted configuration, the light for polymerization first passes through glass before curing the polymer. Because of this there is another efficiency loss in passing through the glass that is related to the wavelength dependent transmittance T of the glass slide at 520 nm.

$$\eta_{glass} = T = 0.93 \quad \text{Equation 4}$$

By combining both of the efficiencies through the optical path in polymerization, an estimation of the input lamp power can be calculated where P is the power required to cure a 200 μm slice of polymer is a given exposure time.

$$Lamp\ Power = \frac{1}{\eta_{optics}} * \frac{1}{\eta_{glass}} * P \quad \text{Equation 5}$$

Another limiting factor in the optical path to be considered, is the digital light processing (DLP) array. Since the light is always in contact with the DLP during steady operating conditions, a steady state heat transfer model for the DLP will be considered. As the DLP is not perfectly efficient in both using electricity to power itself, as well as reflecting light, therefore increased power consumption leads to increased rise in temperature. Given an upper limit input power, the DLP will reach a temperature $T_{array,}°C$ where the DLP will no longer be functional.

To model the temperature at the DMD we used a steady state heat transfer equation (Equation 6) where the temperature of the mirror array ($T_{array,}°C$) is equal to the temperature of the ceramic housing ($T_{ceramic,}°C$) and the rate of heat convection into the array. Where the power in the array($Q_{array,}W$) is the combination of electrical power ($Q_{electric,}W$) from the power supply that controls the mirror position and the illumination ($Q_{illum,}W$) absorbed by the mirrors. $Q_{electric}$ was provided by the manufacturer and Q_{illum} is a percentage ($C, 0.00294\ W/Lumen$) of the incident illumination at the screen (S) where C converts measured Lumens to watts. C was

also provided by the manufacturer and assumes a spectral efficiency of 300 lumens/W for the projected light with an illumination of 83.7% on the active array and 16.3% on the array border and window aperture. Finally, the thermal resistance of the DMD package from the mirror array to thermal couple test point TC3 is measured in $°C$ /W [12, p. 45].

$$T_{array} = T_{ceramic} + (Q_{array} R_{DMD\ package}) \quad \text{Equation 6}$$

$$Q_{array} = Q_{electric} + Q_{illum} \quad \text{Equation 7}$$

$$Q_{illum} = C * S \quad \text{Equation 8}$$

Plotting the resulting we established the maximum illumination we could use before over heating the DMD ($T_{array} > 65°C$) was 25 W on the screen. This equates to an input intensity flux of 4.167 W/cm^2.

When combined with the required optical power to cure the photopolymer in the system's microfluidic devices, a limit to input power can be produced which also limits the system's polymerization speed for a given photopolymer with resin characteristics $\alpha = .0158$, and $D_{c0} = 1.08 * 10^{16}$ as measured. When considering designing the system to use the maximum amount of optical flux from a source before the DLP breaks, as shown in Figure 20 , the photopolymer curing time is estimated as 0.061 seconds.

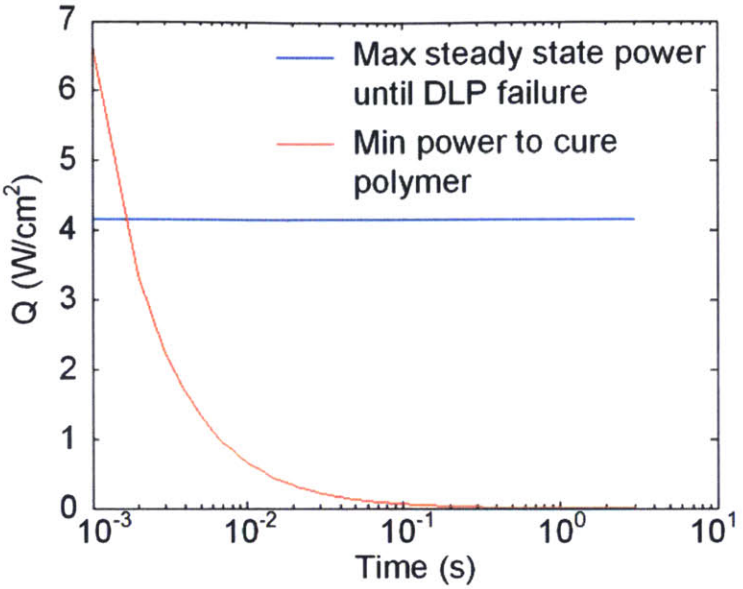

Figure 20. Maximum power input before DLP failure compared to minimum power to cure the polymer for a specified exposure time.

In order to understand the impact of source illumination on the viability of cells used as a substrate in patterning, a lumped thermal heat transfer model is used to model single cells with incident radiant illumination heat transfer q as shown in Figure 21 below.

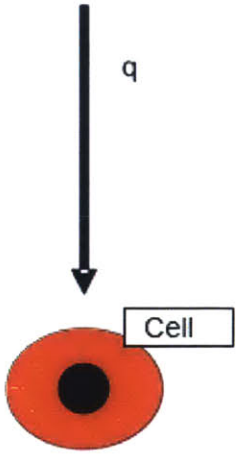

Figure 21. Lumped thermal heat transfer model of the particle.

First as shown in Equation 9, the first law of thermodynamics is used to find the change in internal energy due to a heat transfer flux. Next, this internal energy is equated to two states of heating, the net end heating state U_2 and the beginning state U_1. Next, to find the power required, we relate the power to the net input energy via a time integral. Finally the time integral and the change in internal energy as related to temperature in Equation 13 can be combined resulting in the power needed to raise a lumped thermal mass a given temperature.

$$\Delta U = q + W \qquad \text{Equation 9}$$

$$q = U_2 - U_1 \qquad \text{Equation 10}$$

$$q = \int_0^t \dot{Q}\, dt \qquad \text{Equation 11}$$

$$U_2 - U_1 = m * cp(T_2 - T_1) \qquad \text{Equation 12}$$

$$Qt = \dot{m} * cp(T_2 - T_1) \qquad \text{Equation 13}$$

When a maximum temperature before cell lysing T_2 = 50C and ambient fluid temperature T_1 = 25C is used, along with a cell mass m and cell specific heat c, a relationship of maximum cell input power to time can be deduced as shown in Figure 22.

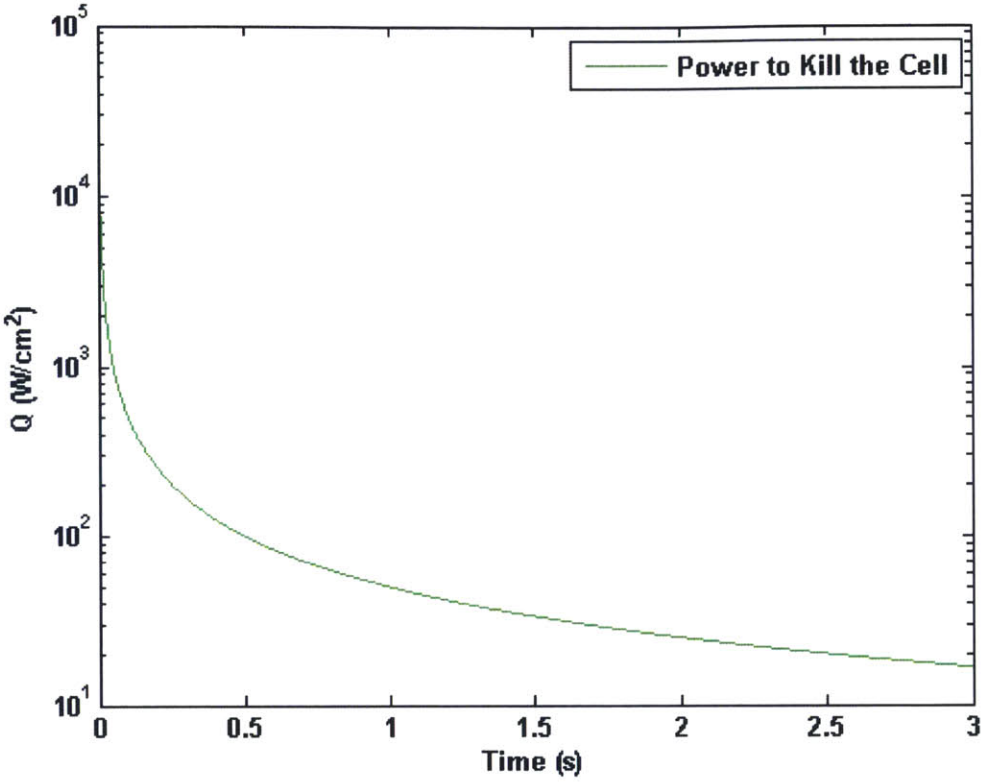

Figure 22. Exposure power that will kill the cell at a specified time.

In the limit that the cell heats to its maximum temperature before lysing, a cooling model must also be incorporated to the net system speed estimate, in order to understand how long the system must wait before polymerizing cells in the neighborhood of other cells that have been heated. Since the temperature is not focused solely on a single cell during the polymerization process, the local area within the channel around the cell is modelled as a conductive infinite fluid, due to the cells size compared to the net channel size of the microfluidic device. Using the infinite plate conduction equations for fluid heat transfer as shown in Equation 14, a graph of realizations of spatial temperature profiles vs. time are plotted in Fig. where T is the spatial temperature at a location x away from the cell, T_i is the initial temperature of the surrounding fluid, T_s is the starting temperature of the heated cell, t is the time after heating has ended, and α

is the thermal diffusivity of the surrounding fluid. The green line as plotted shows the average grid spacing used, therefore creating a bound on where the next cell would logically be placed in a printed array. The temperatures as modelling along this line, can be used to estimate the time needed to wait before the next incident pulse with the maximum or reduced incident illumination power.

$$\frac{T - T_i}{T_s - T_i} = erfc(\frac{x}{\sqrt{4\alpha t}}) \qquad \text{Equation 14}$$

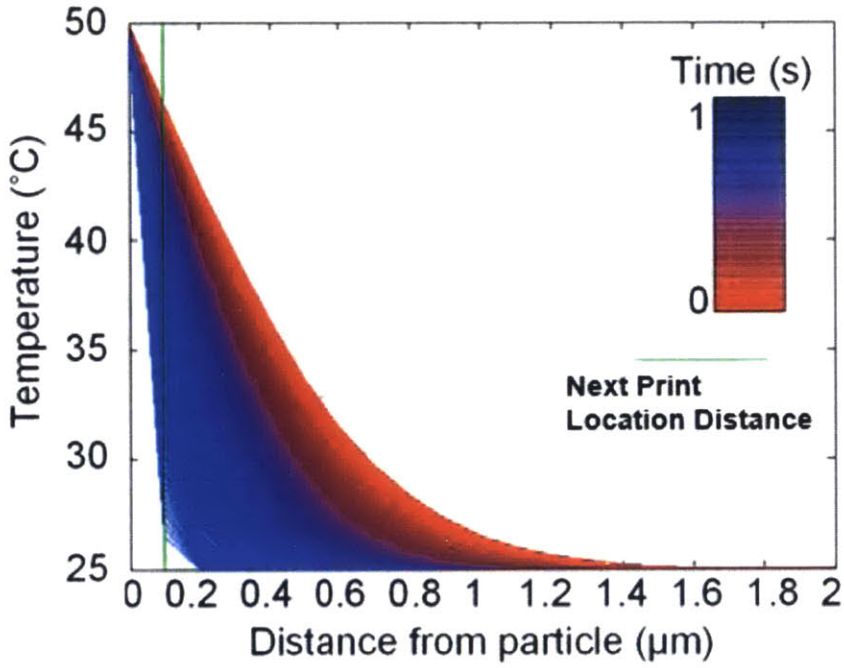

Figure 23. Temperature progression with time at varying distances from the cell.

By plotting the time realizations of radial temperature as shown in Figure 23, a lower limit or waiting time of one second is needed to cool the cell located at any radially spaced printing location down back to its approximate starting temperature before heating. This waiting time can

be shown in the context of the heating time required to heat the cell before it is lysed in Figure 24.

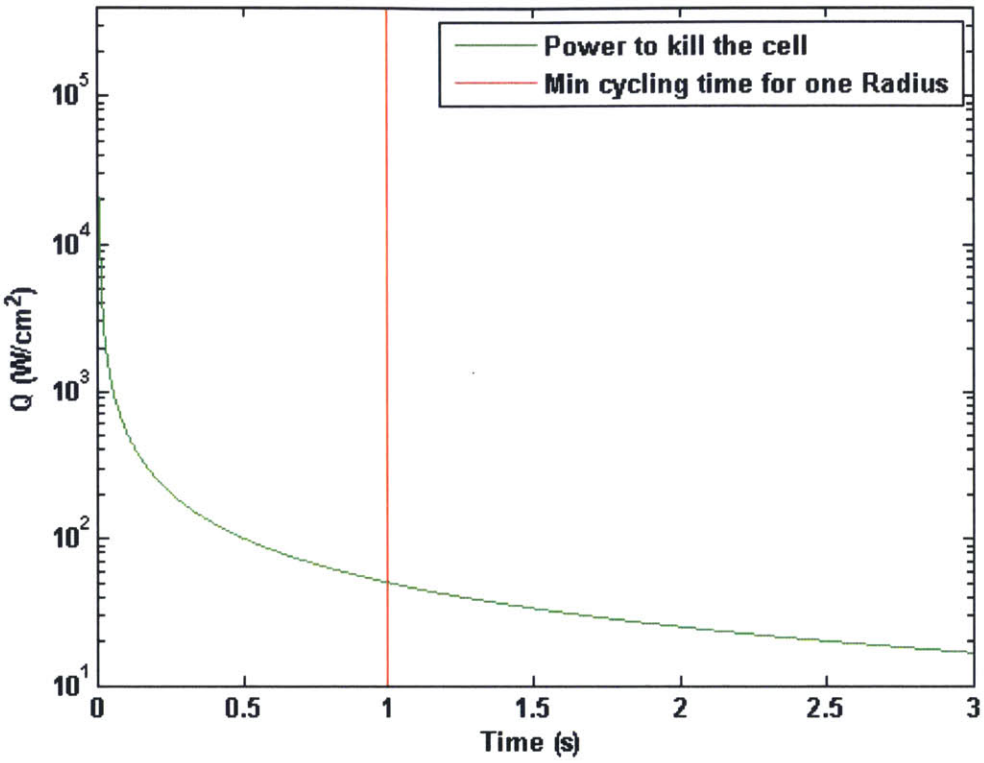

Figure 24. Power to kill the cell from exposure at specified times compared to the cycle time to cool a single exposed cell.

As shown, the limitation of the cell based patterning process, is the power incident on the DLP package before breaking. In theory we could go significantly faster by using slightly less power than the power required to kill the cell, but in this case the DLP would break by overheating. By maximizing the incident power on the DLP package before breaking, the bio-compatible polymer has a curing time of around one second. In polymerizing a single layer of particles at a time the absolute minimum time to finish printing one layer is equal to the polymerization time of one second as shown in Equation 15.

$$Speed = \frac{Layer\ Height}{Layer\ Curing\ Time} = \frac{200\ \mu m}{1\ second} = 200\ \mu/s \qquad \text{Equation 15}$$

3.1.2 Power Analysis and Specification

In specifying the input power to the system, and working with viable materials like cells, we have seen as shown above that the input power to the system will break the DMD first before heating the cell enough to cause death. Because of this, the technique that maximizes the system speed is to maximum the input power without breaking the DMD chip because the magnitude of power per unit of area needed to kill a cell is orders of magnitude higher. Given this analysis, resulting of a maximum power at the DMD of 4 $\frac{W}{cm^2}$, we are able to obtain the input optical system power through multiplication of the DMD chip projected area as shown below in Figure 25.

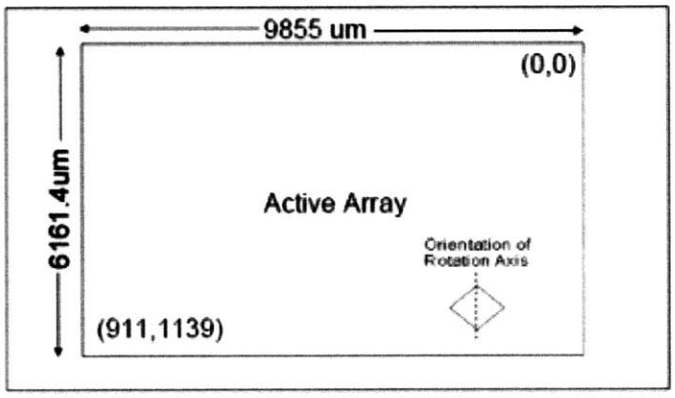

Figure 25. DMD active array dimensions. [12, p. 4]

Since the projection is a circle and the area of the DMD is a rectangle, the optical power must be equally distributed over the circular projection in order to similarly be equally distributed over

the rectangular DMD area. The input optical power can be shown to be calculated as 12.2 W at the input to the DMD chip in the optical path.

$$R_{Projection} = .9855\ cm \qquad \text{Equation 16}$$

$$Input\ Power = 4\frac{W}{cm^2} * \pi * {R_{Projection}}^2 = 12.2 \qquad \text{Equation 17}$$

Compared to the measured intensity value of $0.64\ \frac{W}{cm^2}$, the optical power can be increased over %600 to $4\frac{W}{cm^2}$ at the input to the DMD.

This power is continuous power to the DMD module, as even though lamp has the capability to turn on and off by using a microcontroller, relay, and associated shutter, the power is on the lamp for periods of up to half a minute at times, which eliminated the need for a transient heating response of the DMD due to its large thermal mass.

3.2 Mechanical System Design

In order to print both in two dimensional patterns as well as full three dimensional structures, a mechanical system that allows for precision in positioning samples as well as accuracy in the printing process is integrated into the dynamic lithography system. These mechanical elements work in conjunction with the optical elements above to enable a system capable of flexible photolithography.

3.2.1 Hardware Design for Two Dimensional Patterning

In flexible photolithography and particle encapsulation in two dimensions, the system makes use of microfluidic devices as a means for fluid delivery. In these devices, fluid enters through one inlet and exits through an outlet, by use of a pressure source at the inlet as shown in Figure 26.

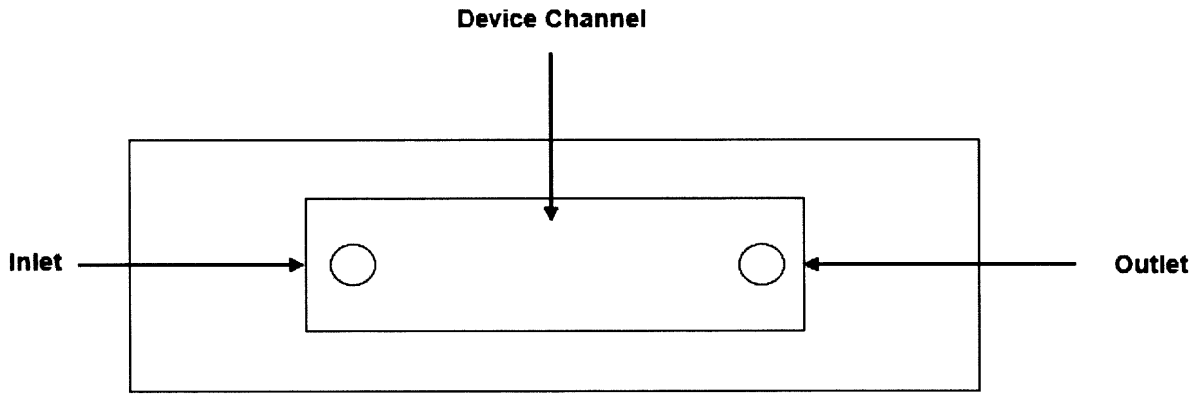

Figure 26. Schematic top view of dynamic lithography microfluidic device

In order to pattern individual parts of the microfluidic channel as well as change the optical focal plane during the lithography process. We have designed a four degree of freedom mechanical coupling that consists of a Thorlabs two axis plus rotation stage with a 10 μm minimum step size in the linear direction and a Thorlabs z stage with a minimum step size of 20 μm shown below in Figure 27.

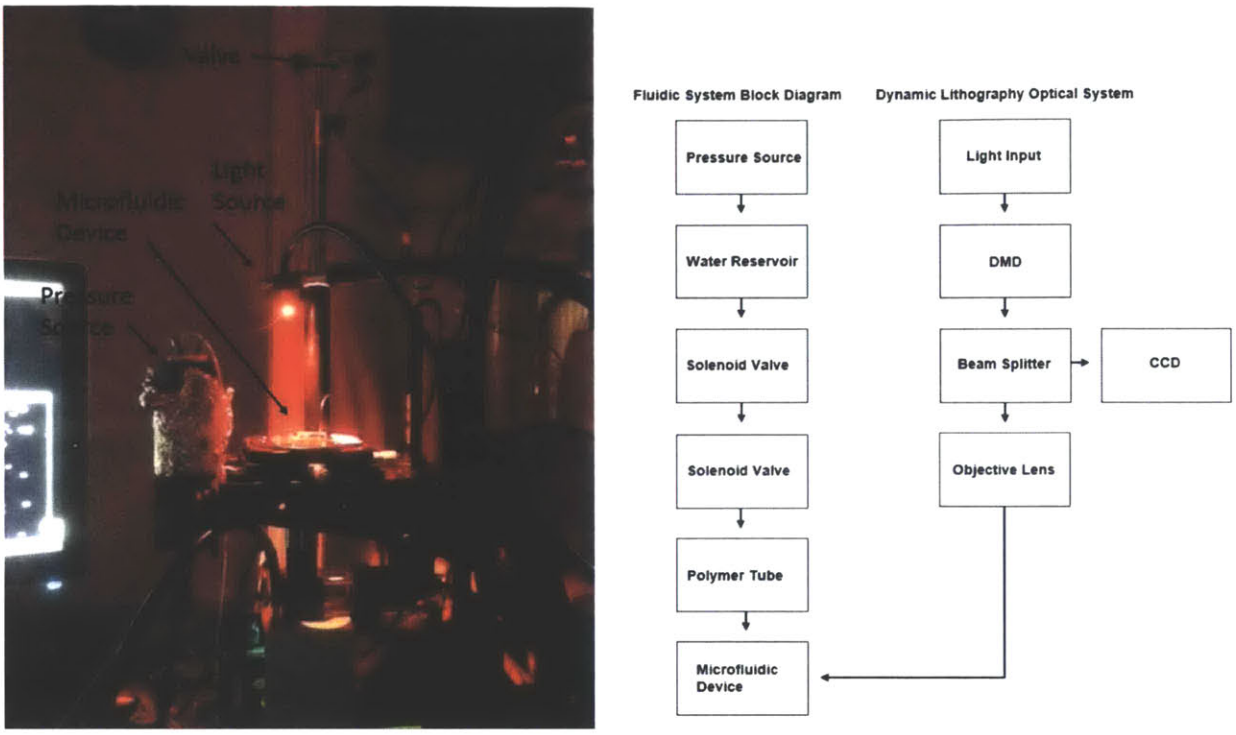

Figure 27. Photograph of the microfluidic pump and device.

These four degrees of freedom allow the optical plane to be correctly focused in the sample and in the correct region of the sample for accurate patterning. The large working range (0 - 160 mm) of the z axis also has the ability to accommodate a variety of sample sizes increasing the flexibility of the lithography process.

3.2.2 Hardware Design for 3D Printing

In order to print complex microstructures, we designed and constructed a system that utilizes stereolithography based techniques and associated hardware. Similar to that of the consumer stereolithography based 3D printer, the Form 1 made by Formlabs as shown in Figure 28, the optical surface is located in a resin containing tank. This tank contains a photopolymer that is polymerized during the printing process. The build platform starts fully submerged in the resin

tank, and the build surface is the bottom surface of the build platform. The optics and scanning laser are contained in a bottom optics chamber, and are used for curing each layer of photopolymer. To demonstrate a micro 3D printing capability with the dynamic lithography system, a similar hardware approach to stereolithography is used on the micro scale as shown in Figure 29.

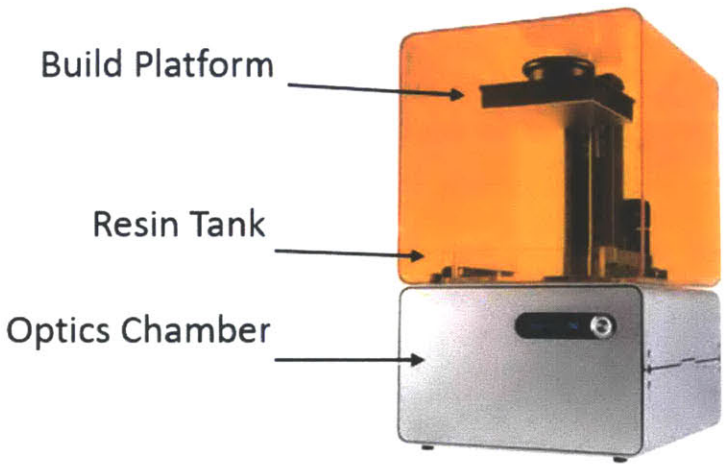

Figure 28. Photograph of Form 1 by Formlabs. [13]

We constructed a resin tank by using conventional fused deposition modelling (FDM) based 3D printing techniques to print a plastic tank body. In order to create a transparent optical surface in the tank, a glass slide was pressed and glued into an inset in the bottom surface of the tank as shown in Figure 29. Lastly, to inhibit free radical polymerization at the bottom surface of the tank, a thin layer of PDMS was cast over the bottom surface.

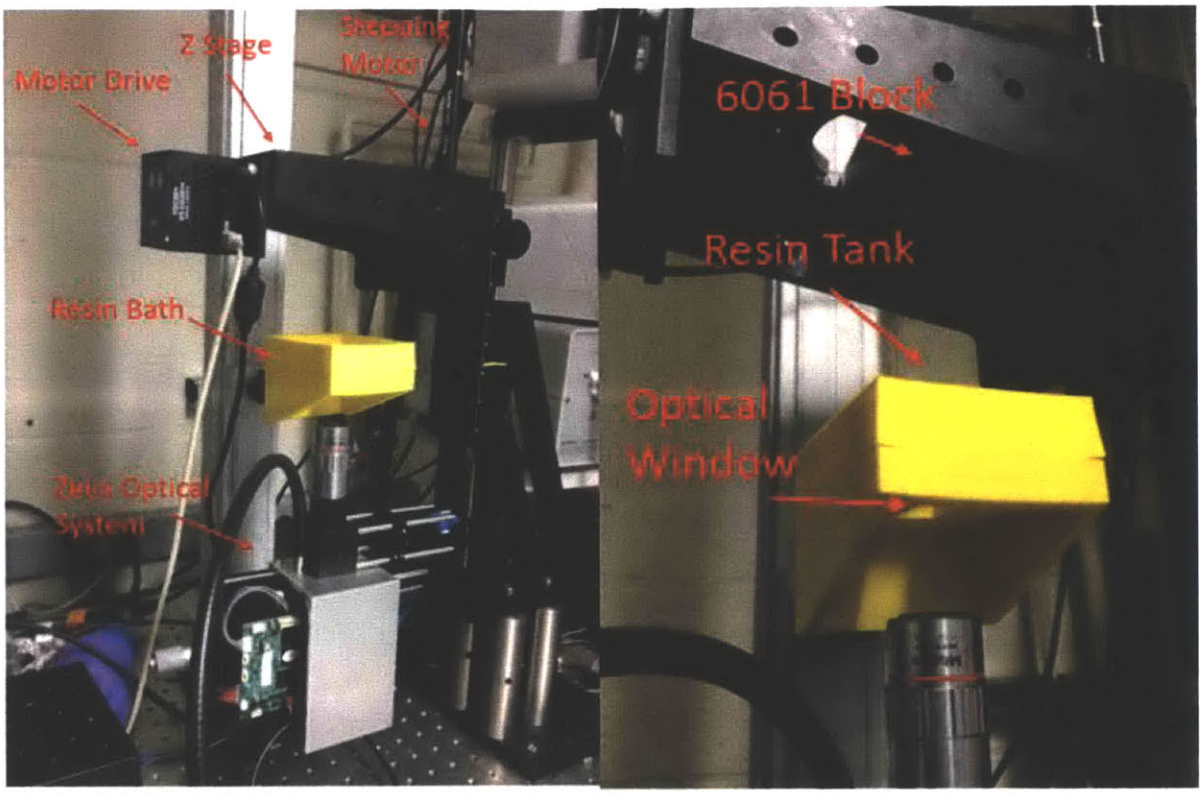

Figure 29. Overview of 3D printing system.

For the build platform, a 6061 aluminum block was machined and lapped flat in order to act as a smooth build surface. This block was then screwed into a Thorlabs optical stage as shown in Figure 29. The optical stage is actuated with a Thorlabs T-Cube piezo stepping drive. This stepping drive enables the build platform to move in and out of the tank during the build process. The last hardware component of the micro-printing assembly is the dynamic lithography optical system, which is the driving system behind the photopolymerization of each layer during the printing process. The dynamic lithography optical system is able to project a pattern for each layer, curing the photopolymer in the layer.

Chapter 4

Software System Design

In order to print complex two dimensional patterns of particles in arbitrary arrangements as well as print microstructures, we have designed software that makes use of computer vision as well as 3D printing techniques.

4.1 Software Design for Two Dimensional Patterning

Building upon previous software for dynamic lithography, a new characterization of polymer kinetics improved the understanding of how particles are anchored during the curing and exposure process. In identifying this relationship empirically, the aim was to improve the accuracy of the dynamic lithography software. Ultimately, the increase in accuracy given the empirical modelling results was not large enough, meriting a move to a stop flow lithography based software.

In order to understand the physical relationship between particle velocity and time for the particle to stop when exposed to light during the polymerization process, experiments were conducted to empirical testing. From using the computer vision based software to track and encapsulation particles on demand, we were able to track the particles in the flow in order to determine their initial velocities when the polymerization process begins. From the point to the polymerization process begins to the point when the particle is fully encapsulated, we are able

measure the time taken, via built in timing functions in software. From these relationships, we were able to plot the time required to anchor a particle during exposure versus the initial velocity of the particle as shown below in Figure 30 and deduce the relationship $y = 248.66x + 251.06$.

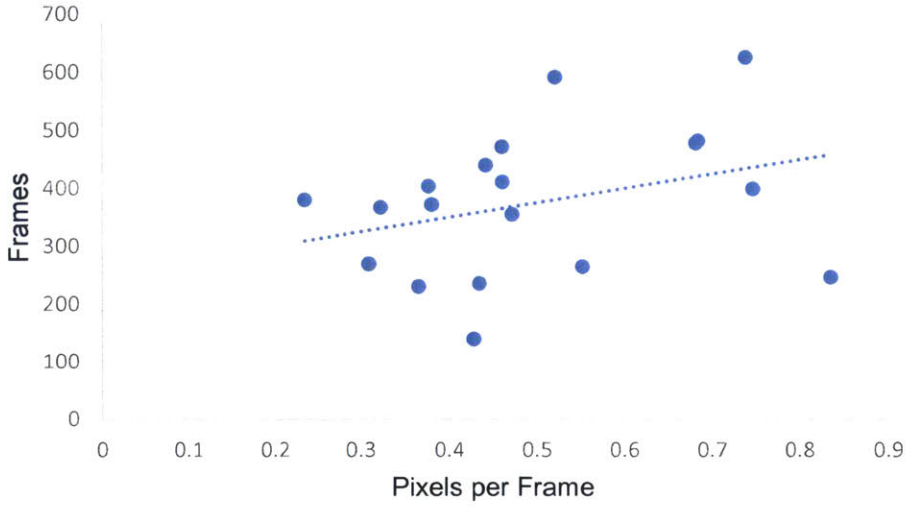

Figure 30. Time to anchor a particle in frames compared to its velocity in pixels per frame.

This relationship is then used to deduce a distance that is required to start the polymerization process, ahead of the print location during particle flow in the microfluidic device channel. If the distance needed to cure the particle based on its initial velocity is known, the software is able to predict when to start curing the polymer so it can be printed in the correct print location during the dynamic lithography two dimensional patterning process. A large spread is observed in the data in part because of the changes in flow speed observed because of particle aggregation, bubble accumulation in the channel, and observed differences in flow across the channel. Without the presence of a large spread, we expect to see a linear profile or velocity versus time to anchor due to the decrease in velocity as the tracked particle is being cured.

The second process, is similar to the dynamic lithography process, but uses techniques commonly used in stop flow lithography. In this sense, instead of the flow being continuous as that in dynamic lithography, the flow is stopped upon each check as shown below in Figure 31.

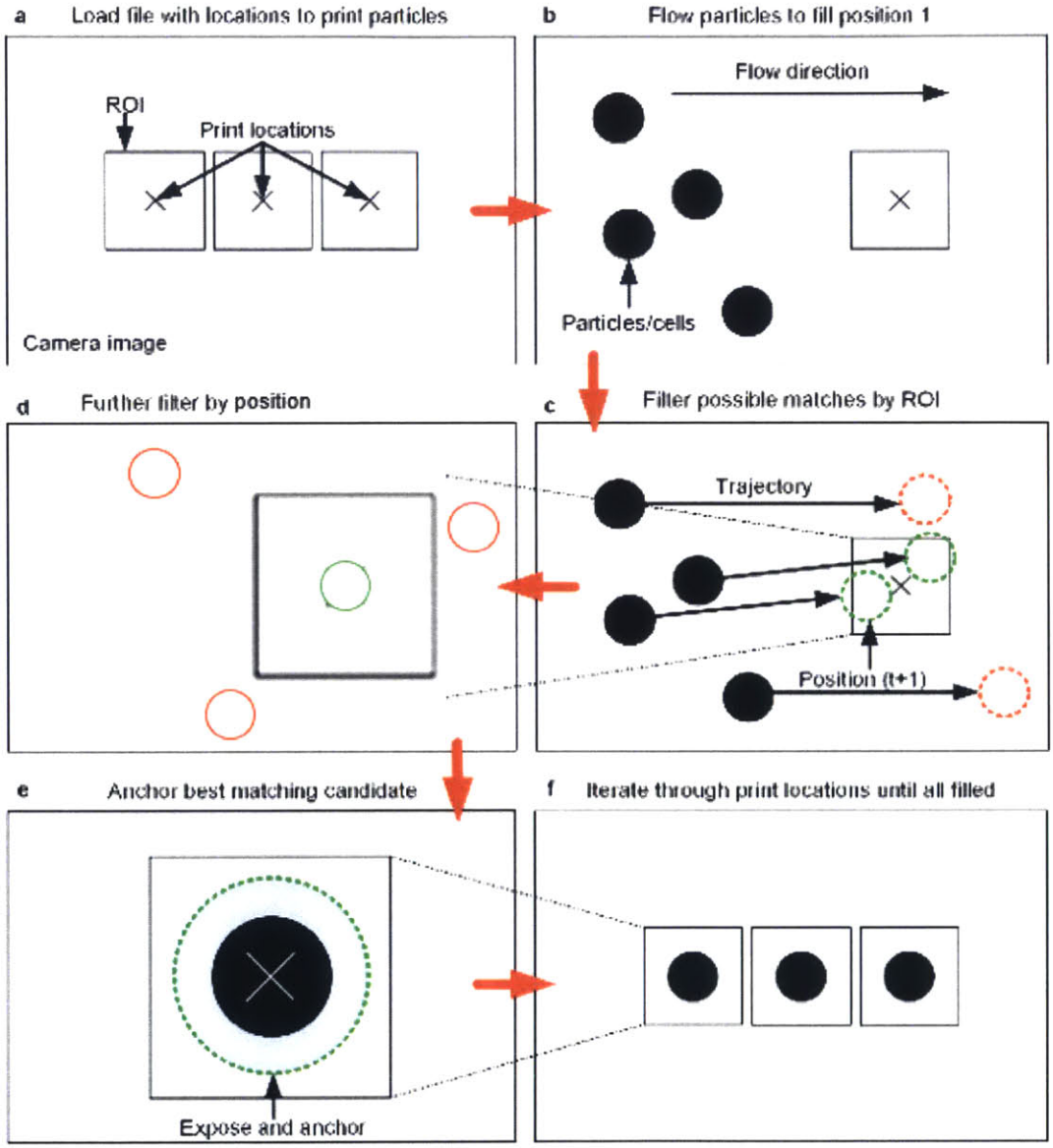

Figure 31. Stop flow based patterning software algorithm. a) Load in the print locations from file. b) Flow particles across the device. c) Stop the flow and identify particles that are close to the print location. d) Select only the best particle according to its position. e) Anchor the particle by exposing a mask onto it. f) Repeat this process for all print locations.

In the stop flow lithography based two dimensional patterning process, the same initial procedure is used to generate a series of print locations and ROIs from a desired user specified mask. Next the flow starts in the flow direction as shown above in Figure 31b. Next, similar to the dynamic lithography process, matches to the desired print location are filtered but this time instead of filtering by angle of attack velocity, they are filtered by position. In this case, when the particle is observed by the software to be within a known desired distance from the print location, on the range of 1-5 pixels as specified by the user, it is photopolymerized and anchored into place by the software. The range of pixels, has an effect on the time to print, with closer locations decreasing the probability of anchoring, therefore increasing the time to print. Once a particle is polymerize the program iterates through the process of flowing for an interval, stopping the flow, checking to see if there are particle and pattern matches, and then continuing the process. After successive iterations of stop flow procedures, the pattern is completely full.

4.2 Software Design for 3D Printing

In order to demonstrate the 3D printing capabilities of the system, the first printing code uses similar printing algorithms to conventional inverse stereolithography based machines. The first step in the micro-printing process starts with an .stl file as shown below in Figure 32 as a micropulley.

Figure 32. STL of micropulley.

Once this .stl file is specified, a set of masks is generated for the flexible lithography process using a web application we have constructed as shown below in Figure 33.

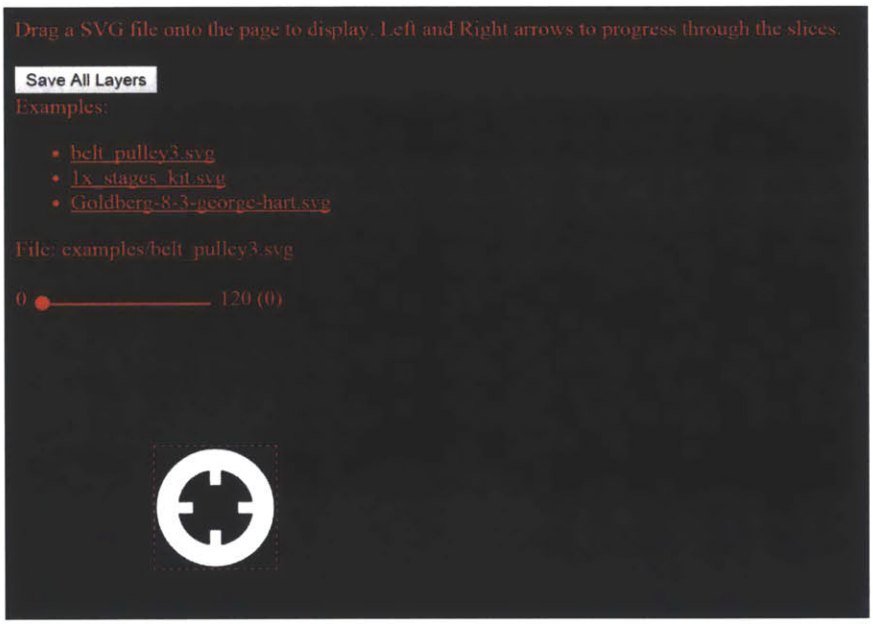

Figure 33. Web application for slicing an STL.

Once the .stl file is imported into the web application, a series of slicing steps occurs as shown below in Figure 34.

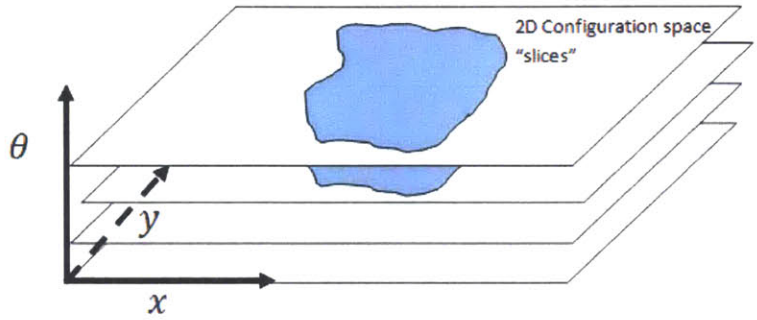

Figure 34. Example of slices taken at various z heights from an STL file. [14]

In the slicing operation, the .stl model has a series of intersecting planes inserted into the model. These intersecting planes, intersect with a series of triangles or vertices that compose the model. By knowing where each triangle or vertices is in three dimensional place, as well as a comprehensive set of planes, we can create a series of intersection curves as shown above in Figure 34. Each intersection plane is inserted in as a single layer, which is a function of the layer height being printed. From these intersection curves, we can then generate a set of contours both open and closed. These closed contours are then used to generate the mask as shown above in Figure 33, as a white pattern, which is a section of the pulley as shown in Figure 32. After each of the masks are computed, the web application exports a series of these photomasks in black and white that are commonly referred to as a stack. This stack of photomasks dictates the exposure pattern of each layer of the 3D printed model during the printing process.

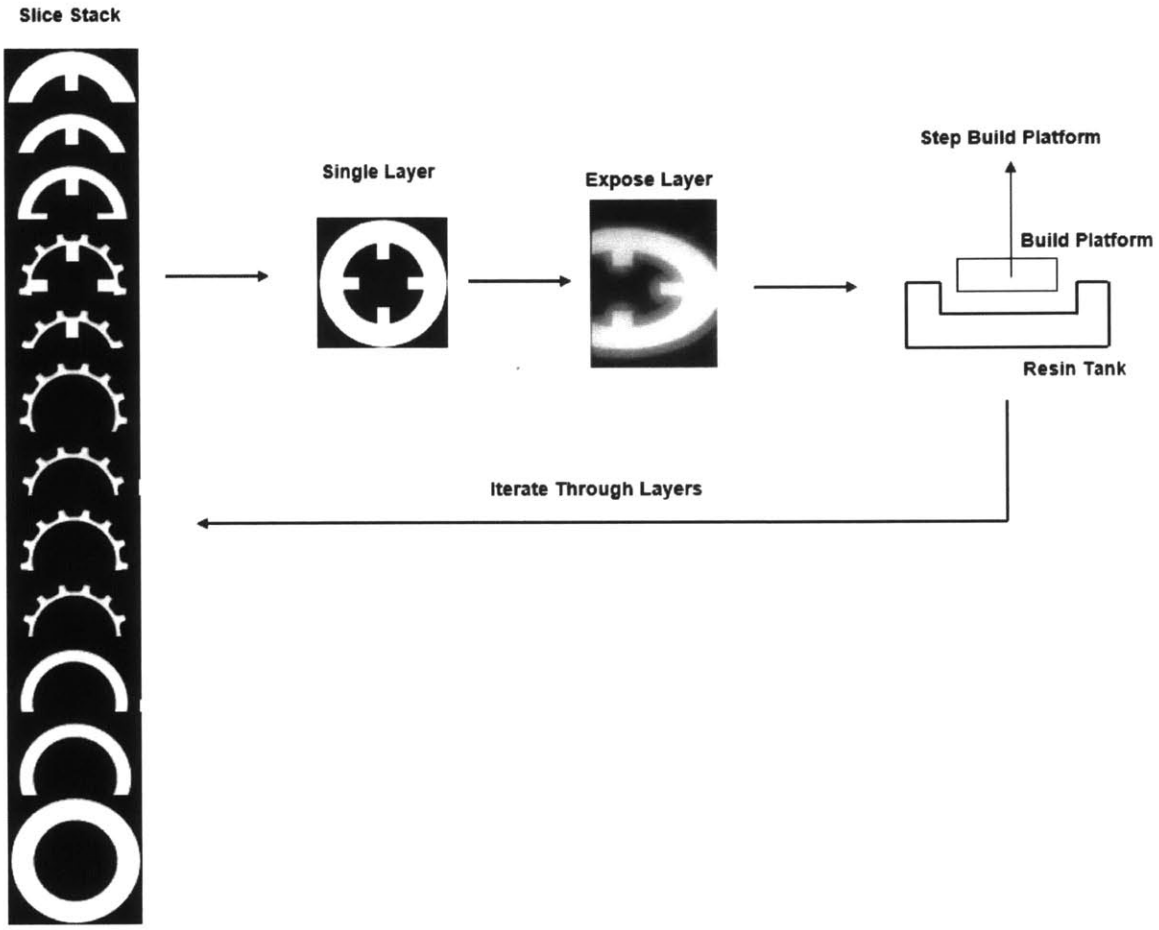

Figure 35. 3D printing process flow diagram

Once the stack of photomasks is composed for a given three dimensional model, the software follows a simple set of steps of exposing the polymer each layer according to the stack of patterns. Upon starting the print, the first mask in the stack is displayed on the DMD for a critical exposure time, curing the specified pattern into the first layer of the part. Next, the software sends a command to the stepping motor on the device's z stage, moving the build platform off the bottom of the window and making room for the next layer of photopolymerization. Finally the next image in the stack is displayed on the DMD and cured forming the second layer. This

process repeats until the model is printed as a successive set of steps of curing and moving of the z axis stage.

Chapter 5

Fluidic System Design

In order to produce two dimensional patterns of particles, we have constructed both a fluid process for anchoring particles as well as a means for printing them. During the printing process particles must be presented to the correct print location at some time interval. We chose to do this by flowing particles across the FOV of the projection system using a microfluidic device. Here we model the flow in that device to understand how it effects the probability of a particle being in the right location.

5.1 Modelling Particle Flow and Delivery

In order to understand how particles behave in flow in a microfluidic channel we have used the Lattice Boltzmann simulation method for computational fluid dynamics simulations. The Lattice Boltzmann method is a particle based model that forgoes the need of trying to solve a simplified version of the Navier-Stokes equation and instead bases its methodology on particle based flow dynamics. The Lattice Boltmann method instead solves a discrete Boltzmann equation in order to simulate the flow of a Newtonian fluid. This simulation is possible through the use of collision based models that allow the simulation of streams and collisions at the microscale within the fluid. From the modelling of the smaller scale particle interaction across a large number of particles, the Lattice Boltzmann method can give insight into the macroscopic flow of a fluid system, such as a particle flow in a microfluidic device [15].

We have constructed a family of Lattice Boltzmann based simulations that have given insights into particle flow in a channel in both organized and unorganized channels, as well as in partially and fully patterned scenarios [16]. In simulation, flow proceeds from the left with a uniform initial speed of 0.1 m/s with a fluid viscosity of $1*10^{-3}$ Pa*s equal to that of water. Particles set up as tracers are initialized in rows of twelve, with a new row of tracers entering the simulation from the left every 18 pixels.

In the first simulations, we learned that given a uniform array spacing larger than the diameter of the particles, there is particle accumulation observed in the gaps between array locations as shown in Figure 36. The accumulation is shown below circled in red, with a tracer size of one pixel. Tracer size is the effective diameter of the circles shown below that are shown flowing in the channel. In flowing particles surrounded by photopolymer in microfluidic channels in the system, accumulated groups of particles act like clots, reducing the flow around them due to a pressure difference that is created. Because of the pressure difference, the flow in the channel changes, leading to inconsistencies in the printing process such as sudden flows of clumped particles, variations in flow speed, and large sudden changes in particle concentrations.

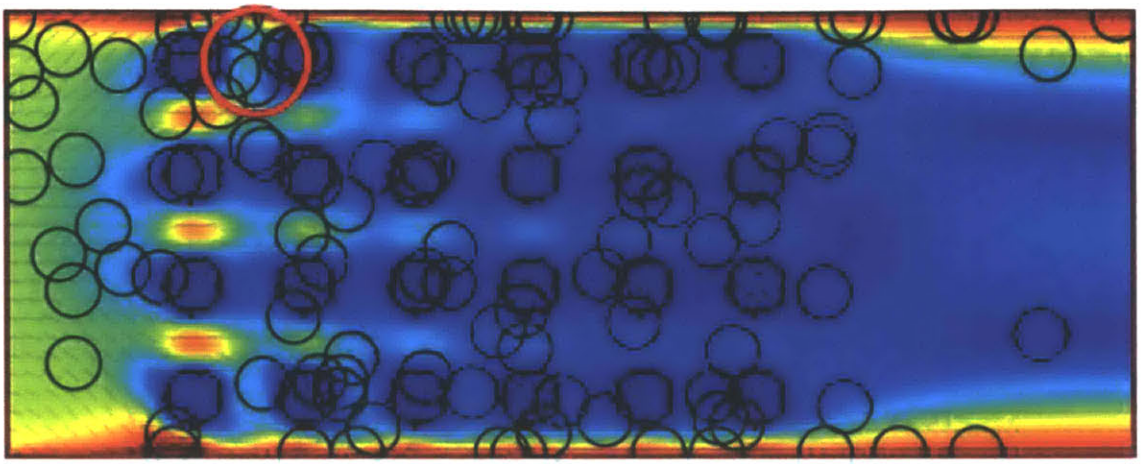

Figure 36. Lattice Boltzmann simulation of flow of tracer particles through a uniform array of pillars. The red circle represents an observation of particles getting caught in flow trap between pillars.

In the second experiment, instead of flowing tracer particles through a fully populated grid, we chose to design a simulation aimed at understanding how the flow changes depending on patterns that are partially filled. As shown in Figure 37 below, the partially filled pattern shows an increase in flow velocity in the part of the channel that is yet to be patterned. This experiment has shown that it is advantageous to fill in the pattern with polymerized particles in such a way that flow is never redirected from previously polymerized particles in front of the print location.

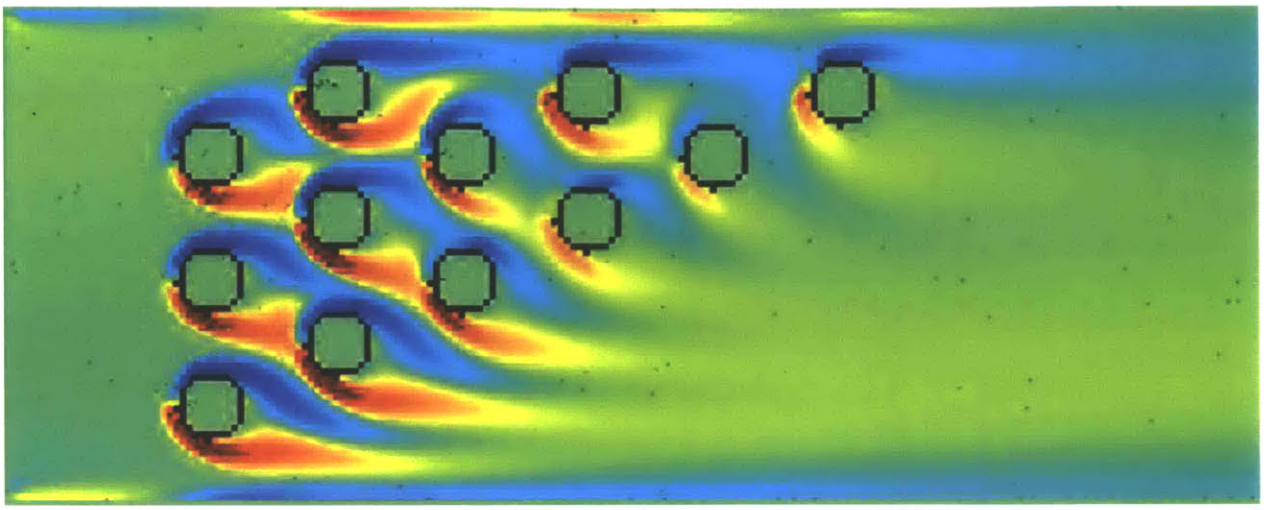

Figure 37. Lattice-Boltzman simulation of flow around alternating rows of varying length.

Lastly, in order to demonstrate a completely filled pattern with optimal spacing, we created an experiment where horizontal lines simulate a filled in pattern with more spacing in the vertical direction than the horizontal direction as shown in Figure 38. In this case, we observed that with a tracer or particle size of one pixel, flow is still freely observed in the dominant flow direction without any obstructions. This flow is critical in completed patterned cell based devices created by the dynamic lithography optical system, because of the need of drug perfusion in the polymerized channels containing cells. Lastly, this experiment is shown to include the effects of a no slip or zero velocity boundary condition as observed in real microfluidic channels, and not so in the previous simulations.

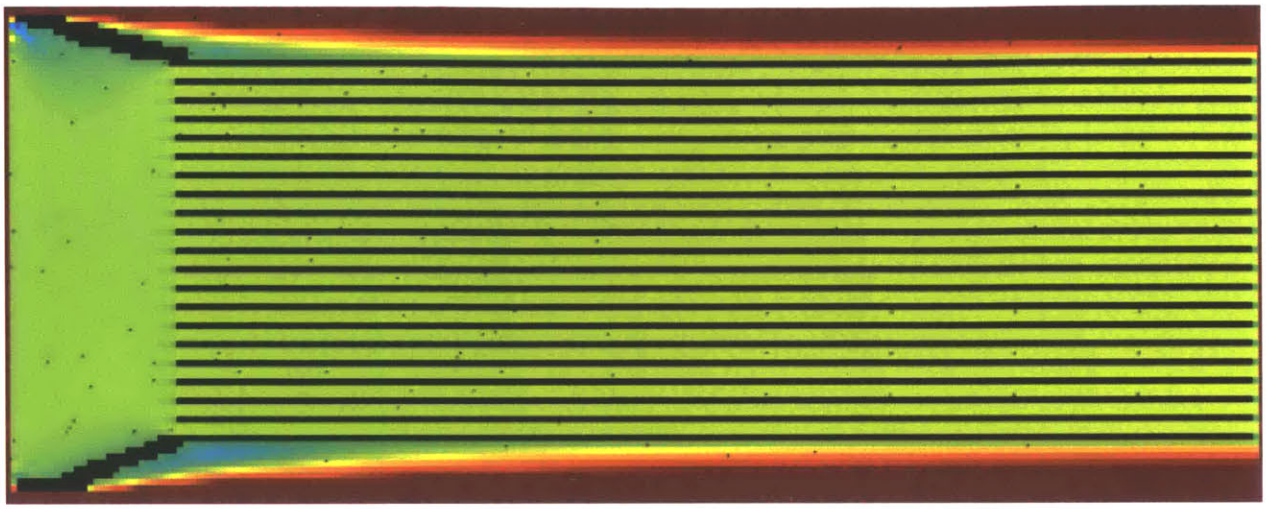

Figure 38. Simulation of flow through channels. The channels represent very closely spaced patterned particles. Edges were added to make the flow resemble what we would expect to see in a stick-slip microfluidic device.

As seen above, by creating an array spacing where the spaces in between patterned particles in the vertical direction is greater than the particle or tracer size, and spacing in the horizontal direction is less than the array spacing size, no clogging occurs and ordered flow is observed in the microfluidic channel. This result is directly used in the creation of masks used to pattern particles, and has a direct correlation with system resolution because of the required spacing in between portions of the mask to eliminate the capability of clogging in between successive print locations.

5.2 Microfluidic Device Construction

In order to pattern particles in two dimensional patterns, we have constructed a process for making microfluidic devices that the system uses [3]. Using methods described by Xia et al., we fabricate PDMS microfluidic devices via soft lithography.

5.2.1 Mold Construction

Molds for making devices in the soft lithography process are made by first using 190 μm Pella glass cover slips. Cover slips are cut into 1-1.5x2.54 mm slices using a glass scoring tool. Once a dozen slices are cut, they are glued in horizontal arrays on an eight inch wafer dish using fast curing cyanoacrylate (CA) glue. Glue is left to dry for twenty minutes and applied with the end of a syringe to ensure coverage is only on the bottom of the coverslips, with no left over adhesive left on the wafer plate itself.

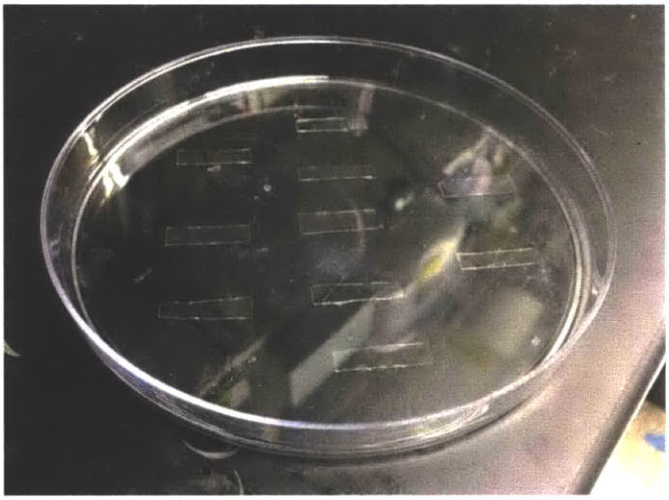

Figure 39. Completed mold for microfluidic devices

5.2.2 Bonding and Device Preparation

Devices are made using Sylgard 184 PDMS resin and curing agents. Resin is mixed in a ten to one volume to curing agent in a 100 ml disposable mixing container until fully mixed and then poured into the mold. Once the mold is filled 1 mm full, the sample is placed in a vacuum chamber which is evacuated to remove all bubbles for thirty minutes. After all bubbles are

removed, the samples are then transferred to an over where they are cured at 85 ºC for one hour as shown in Figure 40 below.

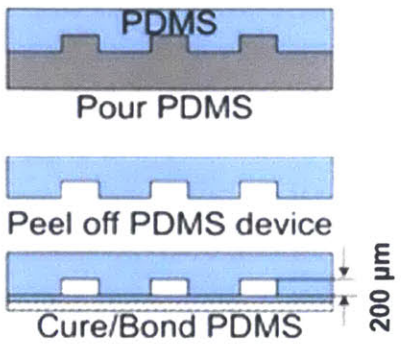

Figure 40. PDMS microfluidic device fabrication process.

Once the devices are fully cured, they are peeled off from the mold, and then cut into individual channeled sections. After these sections are cut, they are then cleaned with isopropyl alcohol and then cut with a 1 mm biopsy punch to create both an inlet and outlet. These sections are then bonded to glass slides using oxygen plasma treatment. During the bonding process, both the surface to be bonded and the glass slide onto which the PDMS device will be bonded are plasma treated for 45 seconds and then immediately bonded by pressing together. After the bond is formed, the devices are put in an oven at 60°C for one hour to facilitate bond formation. The finished device is shown below in Figure 41.

Figure 41. Completed microfluidic device

5.3 Stop Flow Lithography Fluidic Design

In designing a system capable of patterning arbitrary two dimensional patterns of particles in microfluidic devices, flow in the device is controlled with a microcontroller that actuates a piezo valve (The Lee Co. INKX0514300A) using a spike/hold driver (The Lee Co. IECX0501350A) and is paired with the software controlling the manufacturing process.

As shown earlier in Figure 27, at the heart of the fluidic system, a pressure source is connected to a bottle of water, which is then connected to the valve. The valve is controlled via a microcontroller relay system, and is activated from software.

Once the valve is activated, water flows past the valve to the next point in the connecting tube to the microfluidic device. This connecting tube is filled with photopolymer, and is then pumped through the microfluidic device, from the water pressure behind the valve. Since the valve is electronically controlled up to a rate of 1200 Hz, the system can be used for either stop flow lithography based two dimensional patterning or dynamic lithography based patterning.

In preparing the system for stop flow lithography, one of the first steps is adding a polymer stock to the connecting tube. This polymer stock contains particles or cells to be polymerized in the microfluidic devices in the dynamic lithography system. In filling the polymer containing connecting tube with working fluid, the tube is filled using a syringe containing 2 mL of solution at a dilution of 1M particles/mL in order to obtain optimal patterning densities. This concentration was empirically optimized to minimize particle clumping in the fluidic channel after ten experiments of varying concentrations. When the optimal concentration was found empirically through testing, the concentration was quantitatively characterized using a hemocytometer to count particles, and hence determine the particle concentration. Before setting up the cell mixture with live viable cells in the connecting tube, the exposure time of the polymer is checked empirically. First 20 μL of polymer containing cells are placed on a standard microscope slide and then placed on the four axis stage assembly. Once the focal plane is set, a fixed mask projection is focused on the polymer, while simultaneously a timer is set. The timer is then stopped when the polymer cures, indicating the exposure time for the given mix of polymer and particles or cells. While the slide is still on the four axis assembly, the dynamic lithography program is started, in order to set up the system lighting. In combination with adjusting the lighting, the threshold for computer vision based detection is set by using the four axis stage to move a cell or particle into a print location. Once the particle is in the print location, the thresholding tolerance and lighting are both set so that the computer vision both recognizes the particle as well as exposed the cell, anchoring it in place when it is over the print location. After this setup is complete, the connecting tube is ready to be filled with cell containing polymer.

In filling the connecting tube with a biocompatible PEG-DA polymer with the same dilution and cell aggregates, steps must be taken to ensure cell viability. First, all materials are sanitized and then placed in a bio hood, next the cell aggregates are added to the calculated dilution of PEG-DA and then used to fill the PEG-DA containing tube inside a bio hood. Finally, the device to be patterned is injected with first ethanol, then cell media, then finally cell containing PEG-DA. The fluidic assembly is finally reconstructed out of the hood on the four axis stage assembly.

5.4 Polymer Selection for Photolithography

The base polymer used in photopolymerization is polyethylene glycol diacrylate (PEG-DA), which is as hydrogel photopolymer resist. The chemical structure of PEG-DA is shown in Figure 42 below.

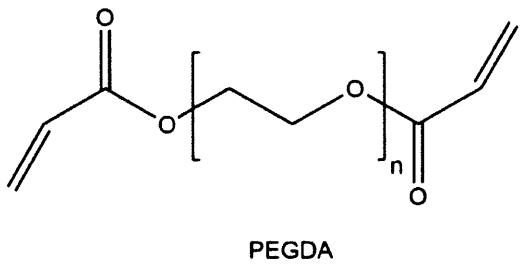

PEGDA

Figure 42. PEG-DA structure [8]

In working with encapsulating cells, we worked to formulate a photopolymer that is both quick to polymerize and capable of ensuring cell viability. Building on work in biocompatible hydrogels by Bahney et al [17]. we formulated a biocompatible PEG-DA hydrogel, capable of polymerizing with exposure times of 0.5 seconds. First, in making polymer for experimentation, a stock solution of 100 mL is selected. First 30 mL of PEG-DA is added to a 100 mL graduated cylinder, and then subsequently 0.00069 g of Eosin Y photoadsorber is added to the mixture and

acts as a dye. Next, 69.9 mL of phosphate buffered saline (PBS) is added to the solution to act as a biological buffer. Finally, 3ml of the photoinitiator, triethanolamine (TEA), is added to the solution [17]. The solution is then mixed in an Erlenmeyer flask briefly, then bottled in an amber bottle and covered in aluminum foil for light protection. The bottle is then sonicated for twenty minutes before use. We have observed that the reactivity of the photoinitiator tends to degrade over time, so for maximum performance, we make fresh photopolymer approximately one hour before each set of biological experiments. In encapsulating polymer particles instead of cells, we use a different photochemistry in order to speed up photopolymerization experiments.

In making the faster photochemistry for polymer particles, we used a white light reactive photo initiator previously demonstrated by Fang et al [18]. In preparation, first 98 mL of PEG-DA is added to a graduate cylinder. Next, measure .006 g of Sudan I, and 2.00 g of phenylbis(2,4,6-trimethylbenzoyl)-phosphine oxide and add these components to the graduated cylinder. Finally, add the solution to an amber photosensitive bottle covered with aluminum foil and mix for 24 hours with a magnetic stirrer and stir bar.

Chapter 6

System Demonstration and Capabilities

6.1 System Performance in Two Dimensional Patterning

By integrating both system hardware and software together, we have been able to demonstrate the ability to arbitrarily encapsulate objects in two dimensional arrangements. This capability has been demonstrated using two different methods: dynamic lithography previously by Ryan Oliver and improved on by stop flow lithography. The improved performance of the stop flow method is determined from patterned arrays of particles and cells. Both cells and polymer beads were used as particles to pattern with varying degrees of success in each case.

6.1.1 Stop Flow Lithography Performance

In the stop flow lithography method, poly methyl methacrylate (PMMA) beads were dispersed in a solution of photopolymer. Particle dispersions were prepared in concentrations of 1 million particles per mL of solution as measured using a hemocytometer. In order to minimize clumping as shown in the dynamic lithography method, thorough empirical experimentation resulted in the calculation of an optimal PMMA bead concentration. Clumping is also minimized by using the simulation results to design an array spacing to minimize particle clumping as seen below in Figure 43. As seen in Figure 43 below and Table 1, the beads are printed in an array with an average mean error in printing location of 11.92 μm with a standard deviation of 4.62 μm. Compared to the dynamic lithography process, the stop flow process is show to produce more

accurate patterning of particles with respect to the desired print location. This inherent increase in both the mean and standard deviation is in part because of only checking positions of the particle to the print location and foregoing the need for understanding of the underlying polymer kinetics behind curing particles in motion.

Table 1. Comparison of dynamic lithography and stop flow lithography performance

	Mean distance from print location (μm)	Standard deviation of distance (μm)	Average gel thickness (μm)	Standard deviation gel thickness (μm)
Dynamic lithography	22	2.5	51.42	27.69
Stop flow lithography	11.92	4.62	16.82	5.24

In the stop flow process, since the flow is stopped and hence the particles are stopped in place before each successive check of the particle and pattern location, the polymer kinetics are not considered since the process is a binary position check. In forgoing this assumption of polymer kinetics modelling and assuming a simple position check, we are able to gain on average 37% in accuracy.

Another improvement over the dynamic lithography process, is that in the stop flow process, the particles have less hydrogel surrounding them as shown in Table 1. Compared the observed trailing and large surrounding hydrogel areas averaging 51.42 μm in the dynamic lithography method, using the stop flow method we were able to obtain an average surrounding hydrogel of only 16.82 μm. This average surrounding distance is the distance from the edge of the particle to

the edge of the encapsulated pillar. This decreased hydrogel leads to less impedance to diffusion and mass transport and hence a higher support for viable cells.

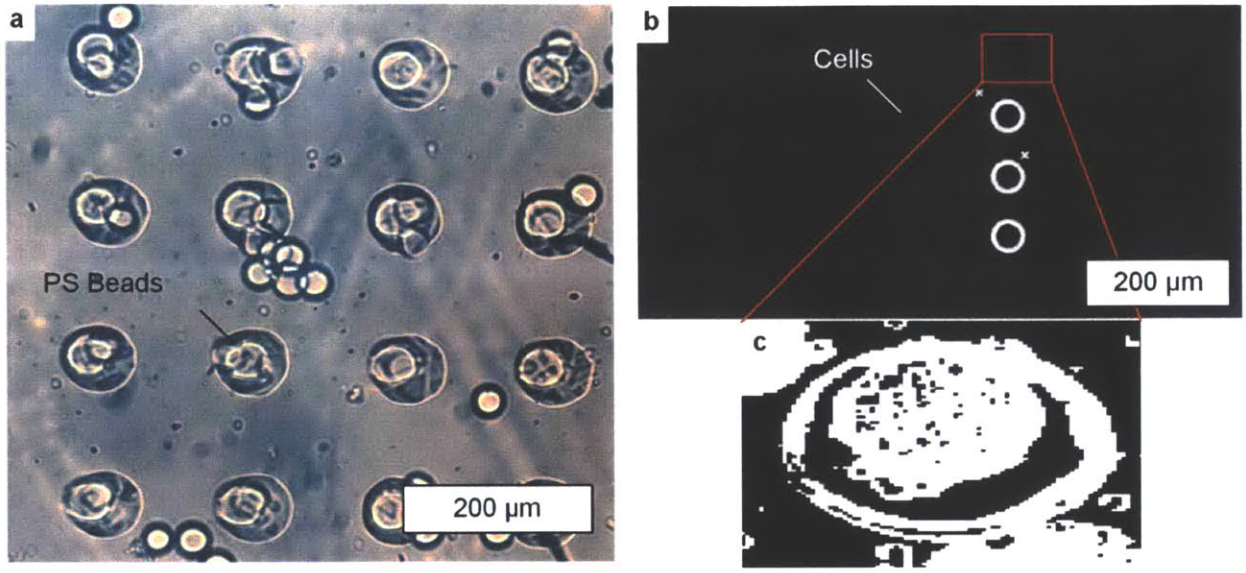

Figure 43. a) Array of PS Beads imaged using 20X after patterning into a 4x4 grid using a 5X objective. b) A column of cells being patterned.

As shown in Figure 43a the completed array is composed of particles at the center of hydrogel polymerized pillars. Spaces are left between the pillars for testing with cells in drug profusion. Spaces in the pattern also help in oxygen and nutrient diffusion, as well as waste diffusion through the hydrogel membrane. In Figure 43b is shown the print locations in the master pattern in the printing of hepatocytes used to dictate the print locations in which anchoring takes place. Enlarged in Figure 43c is the computer vision thresholding operation that is used in checking if the position of the cell during stop flow lithography is close enough to the print location to be anchored in place. Similarly this lack of using polymerization modelling data for the dynamic lithography process, combined with using position based checking, as shown above leads to an improvement in polymerized hydrogel shape, also reflected in the observed system accuracy.

After showing success in patterning of PMMA beads, we moved on to patterning of hepatocyte cellular aggregates.

In printing cellular aggregates, we expected increased accuracy similar to the stop flow lithography with PMMA beads as shown above in Figure 43. As shown above similar problems with particle aggregation cause limitations in print accuracy, as shown by the clumping in the microfluidic channel in Figure 43a. Through optimizing both the pattern and particle concentrations, it is observed that the average clump size in the stop flow experiments is 3 particles while the average clump size in the dynamic lithography process as shown in the MIT logo in the background (Figure 16) is 13 particles. Through empirical observation in printing of cell clusters, aggregation occurred more often in the microfluidic channel perhaps because of the increased size of the aggregates compared to the PMMA beads or due to the cell aggregates' natural affinity to bind together.

Difficulties in aggregation also occurred in the connecting tube that supplies the microfluidic device with a working stock of cells and photopolymer. This aggregation also was prone to cause variations in pressure by building up pressure behind blockages or clots and then causing a sudden release and flow of cell aggregates after the clot is broken up. Not only does the printing concentration drastically increase when a clot breaks up to the point where patterning is difficult, but also does the cluster velocities increase from increased pressure which make patterning very difficult. Furthermore, since the cell working stock is valuable and clusters are hard to manufacture, clots waste cell clusters when they are not patterned. Possible areas of overcoming aggregation include attempting to pattern single cells instead of aggregates or attempting to use Trypsin as a chemical means of decreasing clustering. Other areas of improvement in print

accuracy also are shown by the bubbles present (Figure 44) in the microfluidic channel which leads to both aggregation and deviations from normal flow conditions.

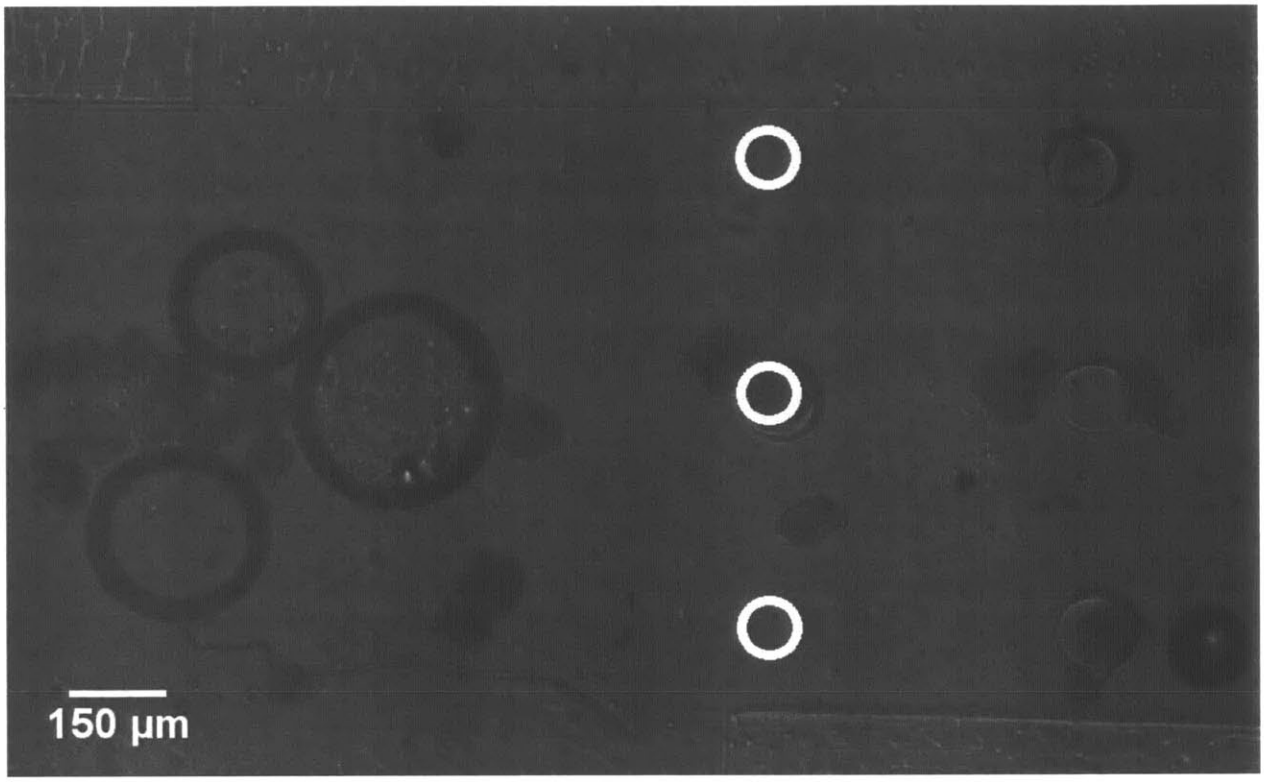

Figure 44. Pattern of two columns of cell aggregates averaging 120 µm in diameter.

Another large limitation to increasing accuracy and demonstration of printing aggregates of cells is the manufacturing process through which the cell aggregates are produced. The cellular aggregates are produced using pyramidal culture mold trays that produce approximately 100,000 aggregates per tray. In culturing cells, the average output in making particle dispersions is approximately 100,000 aggregates leading to a small working solution volume of approximately 100 µL when making solution stocks of 1 million particles per mL. In the future, testing with a higher stock solution volume will increase probability of making completed patterns as well as the ability to make more sophisticated patterns with more print locations. Despite these

observations in the cell printing process, aggregates were successfully encapsulated in hydrogel pillars in a controlled arrayed pattern. Next steps center on printing of single cells with similar accuracies in the stop flow lithography method. Besides printing single cells, another future objective is optimize the system's performance for throughput and patterning speed.

In analyzing the maximum power input as previously shown in chapter 3, we estimated that the limitation in input power to the system is caused by the DLP breaking from too much incident light flux. If we choose to specify our input light source to maximize the system power, but operate right below the condition where the DLP breaks, we arrive at an input light source with an intensity of 4.2 W/cm^2. Using the biologically compatible photopolymer for encapsulation with this upper level system intensity, we find that curing a pillar would result in a critical exposure of 50 ms.

As described by Dendekuri et al [6]. the relationship through which microfluidic channels can be designed is shown below in Equation 18. In designing devices, stop time is approximately equal to the viscosity of the liquid (μ) multiplied by the length of the channel squared (L) and the width (W) divided by Young's modulus of the PDMS (E) and the channel height (H).

$$\tau^t \sim \frac{\mu L^2 W}{E H^3} \qquad \text{Equation 18}$$

As shown by Oliver, when using a pillared microfluidic device with a channel height of 80 μm, channel width of 100 μm, and length of 1,000 μm for the synthesis of particles via stop flow lithography, when using the above design criterion, empirical stop times of 6.48 ms were

observed. In modelling the theoretical maximum output from the dynamic lithography system, we will use this empirical stop time because of its previous measurement in this system. Besides measuring the optimal stop time observed in the system, Oliver also deduced the parameters below besides the pump time and cure times, which are included in Table 2. Once these times are estimated, we can calculate a cycle time for the stop flow process.

Table 2. A description of processing times by task

Station name	Variable	Processing time (ms)	Source
Camera	C_t	11.1	1/fps
Transfer	W_t	11.1	1/60
Demosaic	D_t	6.2	Measured
Detect	X_t	11	Measured
Track	Y_t	10	Measured
Draw	V_t	7	Measured
Transfer	W_t	$16.\overline{6}$	1/60
Project	Z_t	0.02	Estimated
Stop time	S_t	6.48	Measured
Pump time	P_t	0.25	Specified
Cure	H_t	50.0	Modelled

Each of the variables in **Error! Reference source not found.** contributes to the system

Ht Equation 19) [8].

$$t = C_t + 2W_t + D_t + X_t + Y_t + V_t + Z_t + S_t + P_t + H_t \qquad \text{Equation 19}$$

In adding all of the above parameters to deduce the cycle time, we calculate that the system using optimal parameters has a cycle time of 130 ms, with the curing time acting as the bottleneck in

the manufacturing process. In this case 10% of the particles in the FOV are being polymerized, each time the pattern is projected. We hypothesize that this can be accomplished through attempting to check all of the print locations in the FOV at the same time while simultaneously increasing the particle concentration higher and alleviating the clumping problem. As seen below in Figure 45, as calculated by Oliver, with a calculated cycle time of 0.130 s for a particle size of 30 μm and a volume fraction of 0.1, we can expect a throughout of around 10,000 particles per second anchored on the substrate. Based off of physical observations, limitations in optical input power, speed of computer vision in looking over the whole FOV, and lack of optimizing stopping time within the microfluidic device as factors in keeping the rate below 10,000 particles per second. In the current physical system, the stopping time is estimated at 6.2 seconds, with a curing time of 3.0 seconds using the build in LED in the optical system. With these increased components of the cycle time, the current system processing time is calculated as 9.3 seconds, shown below in Figure 45. With the estimated current throughput modelled as about 150 particles per second, there is approximately a 65 fold increase in throughput using the previously modelled results. Discrepancies in current throughput and modelled throughput of the current system are hypothesized to be due to constrictions caused by bubbles, aggregation and clogging in the channel, and changes in flow velocity or stopping time.

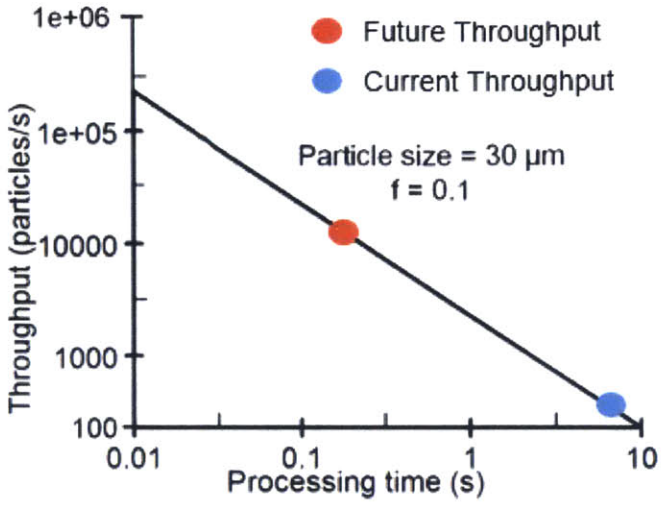

Figure 45. The throughput of the system when only varying processing time. Particle size and volumetric fraction are held constant.

Now that we have demonstrated the expected throughput in patterning a single layer of anchored particles, we now characterize the expected three dimensional resolution as empirically demonstrated by the system and contrast it with existing 3D printing technologies.

6.2 Three Dimensional Printing

In achieving the goal of producing cell laden tissues or eventual functioning organs, the desired capability for photopatterning in arbitrary pattern in three dimensions in necessary. We examine first steps in making a photopatterning system for use in micro scale 3D printing, demonstrating the systems capability to product micro-scale 3D parts.

6.2.1 Performance in Micro 3D Printing

In using the dynamic lithography optical system as a projection engine in inverse stereolithography based 3D printing, we have developed a system capable of micro 3D printing parts as specified by an arbitrary input CAD file. In order to examine the minimum layer height of the 3D parts we have constructed, we have used a Zeiss microscope to optically inspect the printed quality of parts as shown in Figure 46. From our test CAD workflow, we have printed a microgear to demonstrate the micro 3D printing capability of the system.

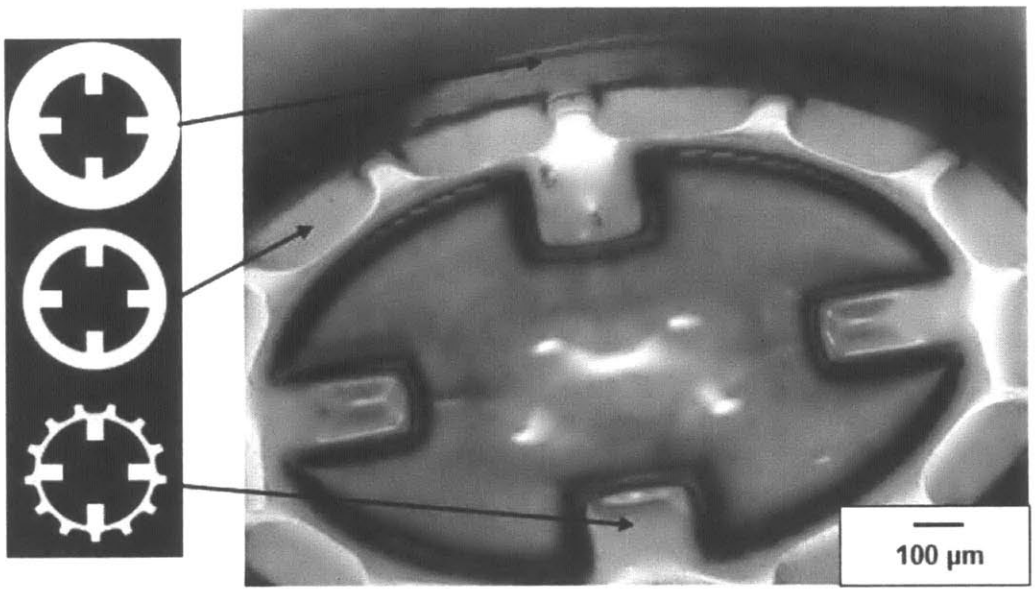

Figure 46. 3D printed part imaged from top with corresponding layers.

By using a Thorlabs TDC-001 micro stepping motor, we have demonstrated that the system is capable of producing 3D printed parts with a minimum layer height of 16.2 µm, owing to a minimum z height resolution greater than most of the conventionally available 3D printers on the market with minimum z resolutions of around 100 µm. Even though we measured a 16.2 µm z height, using the Thorlabs Z85 microstepper, should have the capability to produce 5 µm layers as this is the minimum stepping distance quoted by the manufacturer, but has not been tested yet. Compared to the recently discover continuous layer interface printing (CLIP) technology with a

minimum z resolution of 1 μm and previous work by Prof. Nick Fang in nano-scale stereolithogrpahy with a minimum z resolution of 10 μm, we fall short of observed resolutions. Despite, coming close but falling short of high resolution nano-stereolithography systems, our system is fundamentally different, by adding the ability to encapsulate and organize particles in patterns within each layer, while still retaining the ability to print at the micro scale.

With a minimum planar resolution of 10 μm using hydrogels, overall, considering the 3D printed part's resolution, we have shown to have achieved a minimum resolution of 16.8 μm in the z direction, out of the projection plane of the system. Considering the minimum projection resolution of about 10 μm, and z resolution of 16.8 μm, we have demonstrated a system that performs an order of magnitude better than the industry standard of 100 μm resolution in both planar and z dimensions.

Chapter 7

Conclusion and Future Work

While examining the current capabilities in both 2D and 3D patterning of individual particles, we have identified there is a need for a capability to pattern particles such as cells with single cell resolution with high flexibility. In adapting the dynamic lithography system and method of photopatterning of micro-scale objects in flow, a new stop flow configuration has enabled greater system accuracy, modelling has informed future design goals, implementation and throughput, and preliminary construction of a 3D module has demonstrated micro-scale 3D printing.

In building upon previous work in dynamic lithography, both new hardware and software enabling stop flow lithography resulted in successfully anchoring particles with a mean accuracy of 11.92 μm and a standard deviation of 4.63 μm improving upon the dynamic lithography approach of particle encapsulation. Increased accuracy resulted from implementing a stop flow lithography based method of patterning, improving the tracking capability of the printing software, empirically measuring polymer kinetics, as well as using results from computational fluids simulations. These accuracies can further be increased by substituting the 5X objective for a larger objective. Furthermore, the stop flow method was able to produce a smaller gel encapsulation region around anchored particles due to improved accuracy and achieve an average surrounding gel thickness of 16.82 μm compared to that of dynamic lithography at 51.42 μm. This system has shown the ability to pattern particles in two dimensions and structures in three dimensions with single cell accuracy, with a high level of scalability as shown by the future

ability theoretically pattern 10,000 particles per second. Besides this capability, by using the dynamic lithography computer vision based algorithms and establishing a library of particles to pattern, the system could also theoretically pattern many different types of heterogeneous particles or materials suspended in the same fluid.

In regards to 3D patterning, considerable steps were made towards demonstrating patterning in 3D by both constructing a system capable of micro-scale 3D printing as well as comparing it to conventional micro-scale 3D printers. A module was constructed enabling the ability to use the existing dynamic lithography optical assembly to construct three dimensional micro-scale parts. In comparison, our system achieved a z resolution of 16.8 μm and a planar resolution of 10 μm, compared to Fang's nano-stereolithography with a planar resolution of 32 μm and a z resolution of 10 μm, and CLIP with a z resolution of 1 μm and a planar resolution of less than 50 μm. In producing a 3D printing platform, we have succeeded in manufacturing a demonstrating a platform that can achieve resolutions close to that of the best stereolithography platforms while retaining the ability to print arbitrary arrangements of particles within the polymer matrix. In characterizing the polymer kinetics, we have been able to argue from a power perspective that the speed of the system can be increased by increasing the system input power 4.2 W/cm^2. By increasing the system input power for curing, the polymerization time can be minimized and hence the system cycle time will decrease. With this in mind, the estimated minimum system cycle time in stop flow lithography of 0.130 seconds is calculated and used to characterize a maximum throughput of near 10000 anchored particles per second. With this increased throughput currently limited by exposure time, future design of the system will make use of a higher optical power input, and optimized microfluidic devices for two dimensional patterning.

In anchoring 10000 particles per second, we will be much closer to the grand goal of patterning functional organs, because the increase in speed that drives the scalability of the printing problem.

Future work in micro 3D printing, centers on combining the previous mentioned particle positioning and encapsulation technologies with micro 3D printing capabilities. With the ability to pattern and arbitrarily position particles in photopolymer layers, as well as print in full 3D, we will be closer to developing a capability to print tissues and micro organs or organs on a chip. The process will proceed in a similar fashion to the conventional inverse stereolithography approach previously demonstrated, with the addition of the particle patterning and encapsulation step. Other steps may be necessary to purge with photopolymer without contained particles or in clearing aggregated particles in the channel. Instead of the step in conventional inverse stereolithography of projecting a static mask when curing a single planar layer, the software will implement the flow and particle encapsulation code, resulting in a particle laden arbitrary 3D layer, as opposed to a strictly photopolymer layer. The z stage of the build platform them moves up, making room for the next layer, and allowing the process to repeat. Integration of this voxel based 3D printing platform could eventually lead the way to a new realm of tissue engineering, spanning from integrated organs of a chip to completely artificial organs.

This voxel based printing technology could eventually lead the way to multi-material voxelized structures such as combinations of electrical and biological components, such as build in electrical sensors into living tissues. Limitations in achieving this technology hinges on our ability to scale the manufacturing process to new rates as previously indicated models show, as

well as synthesize new computer vision algorithms capable of tracking broad libraries of printable voxels.

Bibliography

[1] S. V. Murphy and A. Atala, "3D bioprinting of tissues and organs," *Nat. Biotechnol.*, vol. 32, no. 8, pp. 773–785, Aug. 2014.

[2] A. M. Skelley, O. Kirak, H. Suh, R. Jaenisch, and J. Voldman, "Microfluidic control of cell pairing and fusion," *Nat. Methods*, vol. 6, no. 2, pp. 147–152, Feb. 2009.

[3] Y. Xia and G. M. Whitesides, "Soft Lithography," *Annu. Rev. Mater. Sci.*, vol. 28, no. 1, pp. 153–184, 1998.

[4] Y. Zhang, B. K. Chen, X. Liu, and Y. Sun, "Autonomous Robotic Pick-and-Place of Microobjects," *IEEE Trans. Robot.*, vol. 26, no. 1, pp. 200–207, Feb. 2010.

[5] D. R. Albrecht, G. H. Underhill, T. B. Wassermann, R. L. Sah, and S. N. Bhatia, "Probing the role of multicellular organization in three-dimensional microenvironments," *Nat. Methods*, vol. 3, no. 5, pp. 369–375, May 2006.

[6] D. Dendukuri, S. S. Gu, D. C. Pregibon, T. A. Hatton, and P. S. Doyle, "Stop-flow lithography in a microfluidic device," *Lab. Chip*, vol. 7, no. 7, pp. 818–828, Jun. 2007.

[7] B. C. Gross, J. L. Erkal, S. Y. Lockwood, C. Chen, and D. M. Spence, "Evaluation of 3D Printing and Its Potential Impact on Biotechnology and the Chemical Sciences," *Anal. Chem.*, vol. 86, no. 7, pp. 3240–3253, Apr. 2014.

[8] C. Oliver, "Direct-Write Manufacturing and Manipulation of Microparticles, Objects and Organisms." 2014.

[9] L. J. Hornbeck, *Digital Light Processing™: A New MEMS-Based Display Technology.* .

[10] "Digital Light Processing Technology: DLP." [Online]. Available: http://www.opli.net/magazine/eo/2011/news/dlp_tech.aspx. [Accessed: 16-May-2015].

[11] J. R. Tumbleston, D. Shirvanyants, N. Ermoshkin, R. Janusziewicz, A. R. Johnson, D. Kelly, K. Chen, R. Pinschmidt, J. P. Rolland, A. Ermoshkin, E. T. Samulski, and J. M. DeSimone, "Continuous liquid interface production of 3D objects," *Science*, vol. 347, no. 6228, pp. 1349–1352, Mar. 2015.

[12] "DLP4500 | Micromirror Array (>=1 Million) | Advanced Light Control | Description & parametrics." [Online]. Available: http://www.ti.com/product/dlp4500. [Accessed: 16-May-2015].

[13] "Formlabs Form 1+ SLA 3D Printer – Formlabs." [Online]. Available: http://formlabs.com/. [Accessed: 16-May-2015].

[14] "Gamasutra: Matt Klingensmith's Blog - Overview of Motion Planning." [Online]. Available: http://www.gamasutra.com/blogs/MattKlingensmith/20130907/199787/Overview_of_Motion_Planning.php. [Accessed: 16-May-2015].

[15] S. Chen and G. D. Doolen, "Lattice Boltzmann Method for Fluid Flows," *Annu. Rev. Fluid Mech.*, vol. 30, no. 1, pp. 329–364, 1998.

[16] "Fluid Dynamics Simulation." [Online]. Available: http://physics.weber.edu/schroeder/fluids/. [Accessed: 16-May-2015].

[17] C. S. Bahney, T. J. Lujan, C. W. Hsu, M. Bottlang, J. L. West, and B. Johnstone, "Visible light photoinitiation of mesenchymal stem cell-laden bioresponsive hydrogels," *Eur. Cell. Mater.*, vol. 22, pp. 43–55; discussion 55, 2011.

[18] "3d Printing - the Nano-CEMMS Center." [Online]. Available: http://nano-cemms.illinois.edu/materials/3d_printing_full.html. [Accessed: 16-May-2015].